A threshold level of JNK activates damage-responsive enhancers via JAK/STAT to promote tissue regeneration.

John W. Quinn, Mariah C. Lee, Chloe Van Hazel, Melissa A. Wilson, Robin E. Harris*

Arizona State University, 427 E Tyler Mall LSE 229, Tempe, AZ 85287-4501

*Corresponding author

Email: robin.harris@asu.edu

Short title: JNK and JAK/STAT regulate damage responsive enhancers in *Drosophila*.

Abstract

Tissue regeneration requires the directed activity of numerous genes, which are often reused from development. Although the identities of many key factors have been established, how their expression is activated and subsequently coordinated over regenerative time remains unclear. One highly conserved signal central to diverse examples of regeneration is the stress activated MAP kinase JNK. In *Drosophila*, damage-induced JNK signaling promotes expression of multiple genes that direct proliferation, growth and changes in cellular identity. However, how these JNK targets are selectively upregulated in the context of injury, and subsequently expressed in specific patterns responsible for repair is unknown. Our work previously characterized Damage-Responsive, Maturity-Silenced (DRMS) enhancers; regulatory elements that are activated directly by JNK to promote regenerative gene expression. Here we have investigated how the damage-responsive (DR) module of these enhancers are engaged, finding that cell death is entirely dispensable for their activation. We identify JAK/STAT signaling as an additional direct input into DR enhancers downstream of JNK, which acts to broaden DR enhancer activity into the wound periphery where JNK levels are insufficient to promote regenerative gene expression alone. Finally, we demonstrate that a distinct threshold level of JNK activity exists that must be achieved to activate regenerative signaling via DR enhancers, which, alongside input from JAK/STAT, results in their temporally and spatially appropriate expression necessary for regeneration.

Author Summary

Wound healing and regeneration require the activation of multiple genes whose expression must be carefully coordinated to direct the necessary changes in cell division, identity and organ development that promote the restoration of tissue integrity and patterning. The *Drosophila* imaginal disc is a well-established model of regeneration that we have used to better understand spatiotemporal control of reparative gene expression. The response to damage in imaginal discs is primarily mediated thorough the conserved JNK signaling pathway, but how JNK leads to the diversity of gene expression that occurs around a wound is not well understood. Our work previously characterized discrete genomic regions called Damage-Responsive (DR) enhancers that respond to JNK to activate genes of the regeneration program. Here we show that the behavior of these enhancers depends on a threshold level of JNK and that they integrate both JNK and its immediate downstream target JAK/STAT to establish the proper regionality of gene expression, promoting the necessary spread of regenerative signaling around a wound. These findings improve our understanding of how wound patterning is established by discrete regulatory elements that are activated by damage.

Introduction

Regeneration is the ability to repair and regrow damaged or missing tissue and organs, a process that occurs in numerous species across diverse tissue contexts, the equivalent of which often show little to no regenerative capacity in humans (1-3). It has been well established that regenerative growth often relies on the same factors that are required for normal development. For example, FGF8, retinoic acid and Sonic Hedgehog are necessary for both the initial formation of the salamander limb and for its regrowth following amputation, with striking similarities in the temporal and spatial expression patterns of each factor (4). As such, the failure of a tissue to regenerate in many organisms is likely not due to the absence of the necessary genetic factors, but rather an inability to coordinately reactivate their expression after injury. Moreover, there is compelling evidence that regenerative capacity is strongly dependent on the mechanisms that initiate and regulate the expression of factors comprising a regeneration program. Until recently it was unclear how a single gene could be regulated differently during regeneration versus development, but the discovery of enhancers that direct the expression of regeneration-promoting genes specifically in response to damage have provided an explanation (5-7). These types of enhancers have now been identified in diverse organisms and tissues, and often share common features like modularity that guides tissue specificity, promoter compatibility or activity over time, as well as possessing similar signaling inputs and being regulated at an epigenetic level (5-7). The study of these regulatory elements has already led to unique insights into the identity, initiation and behavior of genes that promote regeneration, and to the development of methods to improve regeneration and tissue function in various organisms, including those that normally do not regenerate (8-10). As such, a better understanding of this mechanism is vital.

To explore how regenerative gene expression is initiated and regulated, our lab has used the model of the *Drosophila* wing imaginal disc, a larval epithelial tissue that forms the adult wing structures (11). The wing disc has been used extensively to investigate many fundamental aspects of development (11, 12), and become an extremely powerful platform to study the genetics underlying regeneration (13-15).

Our previous work using the wing disc identified numerous discrete regions of the genome that change in accessibility in response to damage, which occur alongside the changes in expression of nearby genetic factors and therefore likely reflect regeneration-associated enhancers (8, 16). Using a genetic ablation system that we developed called DUAL Control (DC) (16, 17), we focused our investigation on two regeneration-promoting genes, *wingless* (*wg,* the *Drosophila Wnt1*) and *Matrix metalloproteinase 1* (*Mmp1*). Both genes are strongly activated by damage in regeneration-competent early third instar (L3) discs but are only weakly activated in late L3 discs that fail to regenerate (8, 16). We identified enhancers at both loci that are structurally comparable, consisting of separable modules with different functions: a region that drives regenerative gene expression in response to injury/stress signals (damage-responsive, DR), and another region that appears to mediate epigenetic silencing of the enhancer with maturity (maturity-silencing, MS). Together these modules form DRMS enhancers that drive damage-induced gene expression, which subsequently becomes limited in late L3 discs, even in the presence of activating signals (8). Importantly, their modular nature allows the DR and MS regions to be studied independently as separate enhancer and silencer elements, a fact we have taken advantage of to better characterize their behavior in damage contexts. Both the *wg* and *Mmp1* DRMS elements respond to JNK signaling, which acts directly at their DR regions through AP-1 consensus sites (8). We used the damage-induced epigenetic signature of these two elements to identify dozens of regions with DRMS enhancer activity, many of which also bear AP-1 consensus sites, suggesting that multiple genes could be coordinately regulated by this mechanism (16). Furthermore, this mode of activation by JNK signaling and regulation by epigenetic accessibility appears to be important for the progression of regeneration in the wing disc (18), and is common to damage-responsive enhancers identified in other species (5, 6). As such, characterizing the functionality of damage-responsive enhancers and how they control the availability and expression of regenerative gene expression has broad implications.

Crucially, JNK signaling that occurs during normal development, including in the embryo and notum of the wing disc, fails to activate these enhancers or their downstream regeneration-promoting targets (8). This suggests that injury-specific circumstances might exist that allows JNK to induce enhancer activity, or that JNK signaling may not be the only regulatory pathway involved, or both. Therefore, to better understand DR enhancer activation, here we have investigated the potential involvement of additional regulatory factors. We have found that, while JNK signaling is necessary for DR enhancer activation, surprisingly cell death and the resulting downstream signaling events are dispensable. Moreover, we have shown that JAK/STAT, a target of JNK signaling, is necessary for the full activation and proper spatial expression of DR enhancers and their downstream targets. Finally, by isolating JNK signaling from the feedforward mechanisms that arise following cell death, we show that distinct threshold levels of JNK activity exist to control target gene activation: high levels of JNK, such as those found in the center of a wound, are sufficient to activate DR enhancers and their regulatory targets in the absence of additional signaling, while lower JNK in the wound periphery, which is below this activation threshold, cooperates with JAK/STAT signaling outside of the wound to further promote DR enhancer activity. At the lowest levels of JNK, JAK/STAT fails to be activated and therefore only a limited subset of transcriptional targets, including developmentally expressed genes such as *puc*, can be induced. Thus, the different JNK levels generated by a wound, alongside the induction of JAK/STAT signaling surrounding the injury, are coordinately interpreted by DR enhancers to direct the proper timing and spatial activation of different genes required for regeneration, whose activation is limited in the absence of injury.

Results

Cell death is dispensable for activation of the regeneration program via DR enhancers.

To better understand how DR enhancers are activated by damage to initiate regeneration, we examined the behavior of an enhancer at the WNT locus that we and others have shown drives both *wg* and *wnt6* expression upon injury (DRMS^{WNT}, (8, 16, 19)(Fig 1A). To investigate specifically how this enhancer is activated by damage, we used a fluorescent GFP reporter driven by the DR module of the enhancer (*DR^{WNT}-GFP*) (Fig 1A), which has no activity in undamaged tissues and when isolated from the MS region is unaffected by developmental stage (8) (Fig 1B). To induce damage, we use the DC ablation system (16, 17), which is based on a heat shock inducible split *LexA/LexAop* that activates cell death via expression of a constitutively active form of *hemipterous* (DC^{hepCA}) under the control of a *spalt* (*salm*) enhancer in the distal wing pouch (Fig 1C). This cell death triggers the regeneration program in the surrounding surviving cells, which occurs from ~6 h after heat shock (AHS) until ~48 h AHS, with multiple significant regenerative processes represented at the 18 h time point (17) (Fig 1D). Unlike other ablation systems that express a cell death stimulus continuously over an extended 20 - 40 h period (20-22) the DC system generates an acute injury, allowing the events of wound clearance, regrowth, and re-patterning to be characterized separately from ablation. The DC system also includes a heat shock activated GAL4 driver under the control of a pouch-specific enhancer of *defective proventriculus* (*hs-FLP; DVE>>GAL4*), which can be used to manipulate gene expression in the regenerating cells directly surrounding the injury (17)(Fig 1C-D).

We previously found that *DR^{WNT}-GFP* is activated by JNK signaling (8), a crucial early wound response signal essential for initiating the regeneration program following irradiation, physical wounding and genetic ablation (23) . This activation is likely direct, since removal of DNA sequences matching consensus binding sites for the JNK transcription factor AP-1 blocks its activity (8) (Fig 1A). To better characterize this regulatory relationship following damage and as regeneration proceeds, we investigated the expression of *DR^{WNT}-GFP* alongside a reporter for AP-1 that indicates JNK activity (*AP-1-RFP*) from 0 h to 48 h AHS (Fig 1E). Both reporters show significant overlap in expression both spatially and temporally throughout the time course. Neither GFP nor RFP are detected until the 6 h

time point, when both are observed in the same cells (Fig 1E, 6 h arrowhead). By 12 h AHS, there are separate populations of cells that have both fluorescent signals, one positive for the active caspase Dcp-1, indicating cells that have died and are being cleared away (Fig 1F), and another that is negative for Dcp-1, representing cells of the forming blastema that have activated the regeneration program (Fig 1F, arrowheads). This separation of dying and regenerating cells is also observed using a *lexAop-RFP* transgene to label cells undergoing ablation (S1A Fig). At the subsequent 18 h, 24 h and 36 h time points, a significant overlap is still present in the regenerating tissue (Fig 1E), but importantly cells with strong DR^{WNT} enhancer activity are frequently observed to have only moderate or weak JNK activity (Fig 1G, arrowhead). Although we cannot rule out a difference in fluorophore perdurance, the expression of the known JNK target *Mmp1* also shows a similar pattern of overlap with GFP, in which it spatially coincides with, but often does not completely mirror, its strength (S1B Fig), suggesting that the DR^{WNT} enhancer may not be under the sole control of JNK signaling.

Supporting this idea, we noted that JNK signaling occuring during development rather than from damage or stress fails to activate the DR^{WNT} enhancer. JNK is necessary for both dorsal closure in the embryo and thorax closure of notum tissues in the wing disc (24-27). As such, expression of JNK targets, including *puc* and the AP-1 reporter, can be detected in the proximal notum tip (Fig 1H-I). However, *wg* and the DR^{WNT} reporter are not expressed in this region, and neither are several other factors that are known to be directly or indirectly activated by JNK signaling during injury or stress, such as *Mmp1* (28), *Ilp8* (29), *moladietz* (*mol*) (30) or JAK/STAT signaling (31)(Fig 1H-I and S1C Fig). A number of these factors are associated with DRMS enhancers (16). Thus, it is possible that other unknown damage-induced factors are required to activate these targets in addition to JNK. Alternatively, JNK alone may be sufficient, but the level of JNK activity may dictate the activation of developmental versus damage-specific targets.

To test the ability of JNK signaling alone to activate such regulatory elements, we sought to activate JNK and monitor DR^{WNT} activity while blocking other signaling events that occur as a result of damage.

Cells undergoing JNK-induced apoptosis release extracellular mitogens like Wg and Dpp (32, 33), as well as activating multiple pathways in surrounding cells, including JNK itself, via reactive oxygen species (ROS) (34-38). Therefore, to minimize the effects of these downstream events obscuring our analysis, we activated JNK signaling using DC^{hepCA} while blocking apoptosis with a transgene bearing microRNAs targeting the apoptosis-promoting factors *rpr*, *hid* and *grim* (*UAS-mir(RHG)* (39). This transgene blocks cell death downstream of AP-1, but upstream of caspase activation, therefore limiting the signaling events associated with "undead" cells and feedforward JNK signaling (32, 40, 41). This includes the generation of ROS via Dronc/Duox (30, 34, 35), which is significantly reduced although not eliminated in this background (S6D Fig), possibly due to the activity of the Duox maturation factor Mol (36). We found that JNK can still strongly activate the DR^{WNT}*-GFP* reporter even in the absence of cell death (Fig 1J), in addition to activating the enhancer's downstream target *wg* (Fig 1K), and other pro-regeneration JNK targets like *Mmp1* (Fig 1J). Thus, JNK signaling, and the factors immediately downstream of its activation, are the only requirement to trigger the regeneration program via DR enhancers, while cell death and associated signaling events like ROS are dispensable. Moreover, when examined later at 36 h - 48 h AHS, we found that discs expressing DC^{hepCA} and *mir(RHG)* exhibit ectopic growth, resulting in overall larger wing pouch areas (Fig 1L and S1D Fig). This tissue mostly maintains its morphology and polarity, indicative of limited hyperplastic growth, unlike the formation of larger neoplastic tumors created when JNK-induced cell death is blocked by P35 (41). These observations suggest that the pulse of JNK from DC^{hepCA} leads to the production of mitogens such as Wg and Dpp, resulting in overgrowth, but *mir(RHG)* prevents the establishment of the JNK feedforward loop through ROS production, thus inhibiting the persistent expression of these mitogens needed for tumorigenesis. Overall, these data demonstrate that sufficient factors of the disc regeneration program can be activated to form new growth in response to JNK signaling, which occurs at least in part via DR enhancers, even when the normal mechanisms associated with apoptosis-induced proliferation (AiP) and feed-forward JNK signaling are blocked.

Transcriptomic analysis suggests JAK/STAT can regulate DR enhancers.

JNK signaling is sufficient to activate DR enhancers even without cell death. However, JNK is known to activate numerous pathways during regeneration (42), which could also contribute to DR enhancer regulation downstream of JNK. Therefore, to identify whether such factors are involved in addition to direct activation by AP-1 (8), we used whole genome sequencing approaches to identify potential candidate pathways or factors that might act in addition to JNK signaling.

Previously, we used ATAC-seq to characterize changes in chromatin accessibility in damaged and undamaged discs of early and late L3 larvae that might represent DR and/or DRMS regulatory elements (Fig 2A) (16). This work identified 222 regions that become more accessible upon damage in early L3, and 33 that become more accessible in late L3, representing a total of 243 unique putative DR enhancers (16). We re-analyzed the DNA sequences of these regions to identify transcription factor (TF) binding sites that might indicate signaling pathways that regulate these regions in response to damage (see Materials and methods). Searching for motifs that match consensus TF binding sites enriched in the 222 DR regions found in early L3 discs (Fig 2B), or in all 243 DR regions in both early and late L3 discs combined (S2A Fig), identifies several motifs including the chromatin modifier *Trithorax-like* (*Trl*), the DNA binding protein *zeste* (z), which is involved in chromatin-targeted regulation of gene expression, and two early growth response (EGR) family factors, *klumpfuss* (*klu*) and *stripe* (*sr*). The enrichment of these latter two factors is notable, since previous work in the highly regenerative acoel worm *Hofstenia miamia* found that Egr functions as a pioneer factor to directly regulate early wound-induced genes and is essential for activating the entire gene regulatory network necessary for whole body regeneration (43). As anticipated, our search also identified AP-1 (*kay/jra*) binding sites (Fig 2B and S2A Fig), but at a much lower significance level than expected (p.adj = 3.59×10^{-3} in early L3 DR

220 regions, p.adj = 1.82×10^{-5} in all DR regions) despite it being a known regulator of DR enhancers *in vivo*.
221 These observations suggest that although this analysis can identify factors that regulate the chromatin
222 accessibility of DR enhancers, it may not be sensitive enough to identify TFs that control their
223 subsequent activity.

224 As an alternative approach, we performed RNA-seq on discs to identify differentially expressed genes
225 relevant to DR enhancer activation. Importantly, we examined transcriptomic differences that occur in
226 the same conditions as the ATAC-seq experiment (Fig 2A) to identify gene expression changes that are
227 consistent with the regulation of DR enhancers, i.e. those altered upon damage in both early and late
228 L3 discs. Our data identify 570 genes that are differentially expressed upon injury in early L3 discs
229 ($p<0.05$, $Log_2FC>0.4$), with 338 of these upregulated and 232 downregulated (Fig 2C, S1 table).
230 Conversely, late L3 discs have 1406 differentially expressed genes, with 839 upregulated and 567
231 downregulated. (Fig 2D, S1 table). Analyzing these changes using GO term analysis identifies several
232 categories that are significantly altered (Fig 2F-G), including imaginal disc morphogenesis,
233 development and tissue regeneration in early L3 discs, with a more significant enrichment for terms
234 related to immunity, wound healing and defense responses in late L3 discs. Comparing the damage-
235 induced transcriptional changes between early and late L3 discs identifies factors that are uniquely
236 altered by damage at either stage, but also factors that appear to be significantly up or downregulated
237 in both (Fig 2E, S2 table). We find 54 genes that are uniquely upregulated by damage in both early and
238 late L3 discs, which notably includes all three *upd* ligands of the JAK/STAT pathway (Fig 2E-F). The
239 upregulation of JAK/STAT and its essential role in regeneration has previously been described (29, 31,
240 44-48), and it is known to be activated downstream of JNK in numerous stress and injury-associated
241 contexts (22, 29, 31, 46, 49, 50). Thus, we examined how the expression of different factors associated
242 with this pathway change within the RNA-seq data. While the expression of the ligands *upd1*, *upd2* and
243 *upd3* are strongly induced by damage, the pathway components, *domeless* (*dome*), hopscotch (hop)
244 and the transcription factor *Stat92E* mostly remain unchanged (Fig 2H-J). However, known JAK/STAT

target genes such as *Ilp8* (29), *ftz-F1* (51), *mthl8* (52), *chinmo* (53) and *Soc36E* (54) are upregulated by damage in both early and late L3 discs, indicating that JAK/STAT signaling can activate different targets upon injury, and therefore could potentially act as an input into DR enhancers. Indeed, this transcriptional pattern of ligands, pathway transducers and target genes is comparable to that of factors comprising the known DR regulator JNK (S2B-E Fig). Furthermore, although the binding motif for Stat92E (55) is not found to be statistically enriched in the DR regions versus static peaks identified by ATAC-seq (Fig 2B and S2A Fig), a target search shows 50.62% (123/243) of DR regions have consensus Stat92E sites, compared to 68.72% (167/243) with AP-1 sites (FIMO tool $p<0.001$, meme-suite.org). Together, these data suggest that damage-induced JAK/STAT signaling could act to regulate DR enhancers alongside JNK. This is consistent with single cell ATAC-seq analysis that shows genomic regions that change in chromatin accessibility in wounded discs have significant enrichment of both AP-1 and Stat92E binding sites (48). However, these data find the enrichment for Stat92E occurs within a specific subset of cells within the wound, which may explain why it can only be detected with the spatial resolution afforded by single cell analysis versus whole discs ATAC-seq used in our experiments (16).

Notably, the activity of the JAK/STAT pathway in ablated late L3 discs is surprising, since we previously showed that damage-induced expression of a Stat92E reporter (*10XSTAT-GFP*) is diminished in late L3 discs (16). We showed that one reason for this diminished activity is the upregulation of a negative regulator of JAK/STAT, *apontic* (*apt*) (56), in late discs (16). Indeed, our RNA-seq data shows *apt* is upregulated upon damage, as are several other negative regulators of JAK/STAT, many of which are only significantly expressed in late discs (Fig 2I-J). Thus, it is possible that damage-induced JAK/STAT is engaged in late L3 discs via *upd* ligand expression as it is in early L3, but becomes limited by one or more negatively-acting downstream factors.

JAK/STAT signaling coincides with DR enhancer activity.

To test whether JAK/STAT is involved in regulating DR enhancer activity, we first examined the expression of a destabilized GFP reporter for JAK/STAT activity (*10XSTAT-dGFP,* (57), and how it coincides with JNK shown by *AP-1-RFP* (58). Using a time course as before (Fig 1E), we evaluated the changing dynamics of these two pathways in response to ablation with DC^{hepCA} (Fig 3A-D). At 0 h AHS, JNK signaling is limited to the notum and tracheal tubes, while JAK/STAT is present in the hinge (Fig 3A). By 6 h AHS, ablation is evident shown by Dcp-1 staining, alongside JNK activity in the distal pouch (Fig 3B, arrowhead). JAK/STAT activity remains unchanged at this timepoint (Fig 3B). At 12 h AHS, the AP-1 reporter is strongly expressed in the ablated domain, but also appears to be present at weaker levels in the surrounding lateral areas of the pouch (Fig 3C). This pattern of higher distal and lower lateral JNK activity is clearly distinguished at 18 h AHS (Fig 3D-F), and is also observed in our previous time course (Fig 1E). Expression of *lexAop-RFP* and Dcp-1 staining shows this is not caused by different levels of ablation in these regions (S1A Fig). These data support the idea that heterogenous levels of JNK exist in response to damage, potentially leading to the expression of different downstream targets. By comparison, at 12 h AHS JAK/STAT pathway activity is also observed in the JNK-positive cells of both the distal and proximal pouch (Fig 3C). However, by 18 h AHS the expression of the JAK/STAT reporter becomes lower in the distal pouch and upregulated in the lateral regions where there is lower or no detectable JNK (Fig 3D, arrowhead). Quantification of each reporter demonstrates these changes in activity across the distal and proximal regions of the pouch over time (Fig 3G-H). Thus, after 18 h of wound recovery and regeneration, these two pathways occupy mostly distinct populations of cells, with JNK continuing to occur distally within the immediate wound and wound edge cells, and JAK/STAT surrounding this area. By 24 h JAK/STAT signaling has begun to subside and is absent by 36 h AHS (S3A-B Fig). These results are consistent with JAK/STAT signaling being activated after JNK, and show that both signaling pathways have spatially dynamic patterns of expression upon injury. Our observations agree with recently published work that used a different genetic ablation

system (*rn-GAL4/GAL80ts/UAS-egr*) to demonstrate that both JNK and JAK/STAT are activated in response to injury with these similar dynamics (47). It was found that both pathways initially coexist and subsequently resolve into separate populations, with JNK signaling in the center of the wound and JAK/STAT in the periphery, caused by a mutually repressive interaction. This dynamic separation of pathway activity allows JNK-positive cells to temporarily stall cellular proliferation while JAK/STAT promotes it (47). This separation is also observed via single cell analyses (48). We examined the existence of this phenomenon when discs are ablated by DC^{hepCA}, and indeed found a similar pause in proliferation in the high JNK cells at 18 h AHS that is restored by 24 h AHS (Fig 3I-K). However, the surrounding cells with lower JNK do not appear to undergo a similar cell cycle pause (Fig 3I-K). Thus, a similar pattern of wound signaling and changes in proliferation occurs despite the different timing of ablation and recovery imposed by each ablation method, while the acute injury caused by DC also reveals that cells with low JNK levels behave differently than those with high levels.

Having characterized these changes in both signaling pathways following injury, we next examined how the *DR^{WNT}-GFP* enhancer behaves alongside them with *Mmp1* expression as a readout for JNK activity (Fig 3L-N). Our initial time course with the AP-1 reporter showed that the early activity of *DR^{WNT}-GFP* (0 h to 12 h AHS) almost entirely overlaps that of JNK signaling (Fig 1E). However, at 18 h AHS, when JNK activity begins to exhibit a high/low separation and JAK/STAT is observed further out in the wound periphery, we found that the *DR^{WNT}-GFP* enhancer reporter is expressed both in the high-JNK cells with *Mmp1*, and the surrounding lower-JNK expressing cells where JAK/STAT is present (Fig 3L-M). This *DR^{WNT}-GFP* activity continues to span both the JNK and JAK/STAT positive regions at 24 h AHS (Fig 3N), after which it declines alongside that of the JAK/STAT reporter and expression of *Mmp1* at 36 h AHS (S3B Fig). Thus, these detailed time courses examining JNK, JAK/STAT and the DR^{WNT} enhancer show that following wounding, the DR^{WNT} enhancer becomes activated by JNK in the wound center, where it then expands to the wound periphery as lower JNK and JAK/STAT signaling become

subsequently activated. These dynamic patterns of overlap suggest that both JNK and JAK/STAT can regulate DR^{WNT} activity, and potentially do so as the wound is stratified within the first 24 h after injury.

JAK/STAT acts directly on DR enhancers to induce their activity in the periphery of the wound.

To test whether JAK/STAT is required to promote DR enhancer activity, we manipulated JAK/STAT pathway elements during disc ablation and examined the effects on the DR^{WNT} reporter. Expressing an RNAi that targets *Stat92E* (*UAS-Stat92E*^{RNAi}) in the pouch significantly limits the expression of *DR*^{WNT}*-GFP* throughout regeneration (Fig 4A-B). The damage responsive enhancer of *Mmp1*, *DR*^{Mmp1}*-GFP*, shows a similar reduction in activity (Fig 4F-F' and S4A-B Fig). Importantly, we noted that the intensity of both GFP reporters is reduced in the center of the wound where high levels of JNK occur, while at 18 h when JNK becomes separated into higher/lower regions and JAK/STAT is induced in the proximal pouch, the knockdown of *Stat92E* eliminates *DR*^{WNT}*-GFP* expression in the cells where JAK/STAT normally occurs (Fig 4C-C'). This knockdown does not affect cell death (Fig 4C-C') or the level of JNK, shown by the AP-1 reporter (Fig 4D-D'), suggesting that JAK/STAT contributes to DR^{WNT} activity downstream of JNK. Together, these observations suggest that, while higher JNK signaling can activate the DR^{WNT} enhancer alone following damage, JAK/STAT is required for normal levels of damage-induced DR activation in the proximal pouch where JNK is lower.

To further test this idea, we examined the behavior of another DRMS enhancer identified in our accessibility data set (16), which is located between two genes, *Tdc1* and *Tdc2*, that are among the most strongly upregulated upon damage in our RNA-seq analysis (S1 Table). A GFP reporter for this region (*DRMS*$^{TDC1/2}$*-GFP*) has 3 sites matching the AP-1 consensus sites found in DR^{WNT} that are necessary for its activation (8) and exhibits damage-responsive, maturity-silenced behavior (16) (S4C Fig). However, unlike the $DRMS^{WNT}$ or $DRMS^{Mmp1}$, this region does not contain any consensus Stat92E

binding sites (although the reporter construct includes short flanking sequences of the genomic region that bears one site S4C Fig). Upon ablation, the *DRMS*$^{TDC1/2}$*-GFP* reporter has a smaller activation footprint than those at the WNT and *Mmp1* loci, and is unaffected by *Stat92E* knockdown (S4D-E Fig), suggesting that JAK/STAT signaling does not act on this enhancer to promote its expression.

Together, these data suggest that JAK/STAT signaling can augment the activity of some DRMS enhancers following damage, particularly in regions with lower levels of JNK, while the existence of Stat92E binding sites suggests that this regulation acts directly rather than through an intermediate. To confirm this possibility, we generated a DR^{WNT} reporter with the three identified consensus Stat92E binding sites removed (*DR*$^{WNT\Delta STAT}$*-GFP*, Fig 4E-E' and S4F Fig). The absence of these sites significantly reduces reporter activity in intensity within the wound and eliminates it from the wound periphery (Fig 4E-E' and S4G Fig), phenocopying the knockdown of *Stat92E* (Fig 4C', D' and F') and suggesting that the JAK/STAT pathway is likely a direct input in the WNT enhancer via Stat92E, similar to AP-1.

Finally, to assay changes in regenerative capacity we examined the size and completeness of adult wings following DC^{hepCA} ablation in the presence *Stat92E* knockdown in which lateral DR activity is reduced. We found that regeneration was impaired, indicated by reduced wing phenotype scoring (16)(Fig 4G), and wing area (Fig 4H). Thus, Stat92E is required for proper regeneration at least in part by promoting activity of regenerative gene expression via DR enhancer activity following injury.

Ectopic JAK/STAT is insufficient to activate DR enhancers.

Although JAK/STAT signaling is necessary for full and spatially appropriate DR enhancer activity downstream of JNK, the question remains as to whether it is sufficient to induce their activity in the absence of JNK. To test this, we overexpressed *hop* in the distal pouch (*salm-GAL4*, *UAS-hop48a*) to ectopically activate JAK/STAT signaling. Although this expression activates *10XSTAT-dGFP* in the

pouch (Fig 5A), it is insufficient to activate the *DR^{WNT}-GFP* reporter (Fig 5B). This is despite the presence of low levels of cell death caused by *hop* overexpression (Fig 5A-B). We repeated this experiment with different GAL4 drivers that express throughout the whole pouch (*rotund-GAL4*) or in both the pouch and the notum (*hh-GAL4 and ptc-GAL4*). These drivers activate JAK/STAT signaling (S5A Fig and S5C Fig), and even can lead to the formation of ectopic pouch tissue (S5C-D Fig) as described previously, (50). However, they do not activate the DR^{WNT} enhancer (S5B Fig and S5D Fig) or other JNK targets such as *Mmp1* (S5A-B Fig). The use of a stronger *hop* construct (*UAS-hopORF*) leads to significant cell death, which in turn triggers JNK signaling shown by *Mmp1*, and thus JAK/STAT and *DR^{WNT}-GFP* expression (S5E-F Fig). As such, these data show that JAK/STAT signaling alone is not sufficient to activate DR enhancers, but rather it is required to fully promote and maintain their activity following their initial activation by JNK.

Since JNK is a prerequisite for DR enhancer activation, we wondered whether JAK/STAT could alter DR enhancer behavior in different contexts where JNK is already present: either following damage or during normal development. We first tested ectopically expressing *hop* during ablation and found that this additional JAK/STAT signaling does not significantly alter *DR^{WNT}-GFP* expression (Fig 5C-E). These data suggest that JAK/STAT is not limiting for promoting DR enhancer activity following genetic ablation. Next, to examine whether JNK occurring during development can activate *DR^{WNT}-GFP* when JAK/STAT is introduced, we expressed *hop* in the notum where JNK acts to promote thorax closure but JAK/STAT is absent (24, 25, 59), (S1C Fig). We used two different tissue-specific GAL4 drivers, *patched* and *pannier*, (*ptc-GAL4* and *pnr-GAL4*), both of which express in domains that overlap the activity of JNK in the notum (Fig 5F-G'' and S5G-H Fig) and can activate the 10XSTAT reporter in response to *hop* (Fig 5F'' and G''). Even with the activity of both signaling pathways, the *DR^{WNT}-GFP* reporter failed to activate (Fig 5H-I'), suggesting that JNK expressed during development is not sufficient to activate DR enhancers even with the addition of JAK/STAT. By contrast, JNK during injury initiates enhancer activity, while the simultaneous induction of JAK/STAT acts to expand their

expression into the wound periphery. Since we have shown that cell death is dispensable for DR enhancer activity (Fig 1), it is unlikely that injury-specific factors are responsible for this context-dependent activation, thus raising the possibility that the strength of JNK signaling might crucially inform DR enhancer activation.

A threshold level of JNK activity is required to initiate the regeneration program via DR enhancers.

To test whether the absolute level of JNK signaling activity might be a factor in whether DR enhancers and their pro-regeneration targets are upregulated, we developed a method to induce different levels of JNK activity in the wing disc that, unlike the dynamic changes within a wound, occurs in a more steady-state condition and thus can provide a clearer understanding of pathway/enhancer interactions. As *UAS*-driven transcription by GAL4 can be altered by temperature (60), we modulated JNK levels by expressing a wild type *hep* transgene in the distal pouch (*salm-GAL4, UAS-hep*^{WT}) at 22ºC and 30ºC, corresponding to JNK^{Low} and JNK^{Med} levels, and a constitutively active *hep* controlled by temperature sensitive GAL80 (*salm-GAL4, UAS-hep*^{CA,} *GAL80*^{ts}) which is activated by temporary culture at 30ºC to generate a JNK^{High} level. We used *AP-1-RFP* as a readout for JNK activity (58) and blocked cell death with *mir(RHG)* to limit ROS production, which is an essential signal required to promote the spread of JNK via feedforward activation (22, 30, 61). Indeed, ROS is only minimally produced under these conditions versus ablation (S6A-C'' Fig), and JNK activity is consequently contained to the distal pouch (Fig 6C). Expression of the JNK target *mol* that is important for ROS production is also unchanged (S6E-F Fig). The different levels of JNK activity in these experiments were confirmed using quantification of *AP-1-RFP* via fluorescence intensity (Fig 6A) and qRT-PCR of transcript expression (Fig 6B). With this setup, we examined expression of JNK targets known to be expressed in the notum during development (*puc*) or upregulated during regeneration (*Mmp1*, *Ilp8*, *wg*, and *Stat92E*), as well as the DR enhancer reporters of *wg* and *Mmp1* (Fig 6C). Our results show that JNK^{Low} fails to activate

JAK/STAT signaling, *DR^{WNT}-GFP* or the other regeneration-specific JNK targets we examined (Fig 6C). By contrast, *puc* is activated by JNK^{Low} (Fig 6C), suggesting that it may have a lower activation threshold than the other targets tested. A more moderate level of JNK signaling (JNK^{Med}) similarly fails to activate JAK/STAT and the other targets tested except *puc*, but weakly induces *DR^{WNT}-GFP* and *DR^{Mmp1}-GFP* reporters and their target genes (Fig 6C). Conversely, high levels of JNK signaling (JNK^{High}) activates JAK/STAT, but only outside of the JNK expression domain (Fig 6D), consistent with the non-autonomous upregulation and autonomous blocking of JAK/STAT by JNK in a late wound (47). Under these conditions, the DR reporters and all the regeneration-specific targets we examined, including *wg*, *puc*, *Ilp8* and *Mmp1*, are strongly upregulated within the JNK^{High} domain (Fig 6C). However, unlike in a wound, they are not upregulated outside of this domain where JAK/STAT is activated, likely because blocking cell death prevents the spread of JNK beyond this initial expression domain. This prevents the formation of a region in which lower JNK and JAK/STAT overlap, which we have shown is required for DR enhancer activation. Thus, together these experiments demonstrate three important findings: 1) a particular threshold level of JNK is needed to activate JAK/STAT signaling, which in steady-state conditions (and late wounding) becomes exclusively non-autonomously expressed, 2) at high levels of JNK, DR enhancers and their downstream pro-regeneration targets can be activated, and 3) when the spread of JNK and the subsequent formation of different levels is prevented by blocking cell death, the activation of DR enhancers and targets outside of the high JNK domain does not occur, even in the presence of JAK/STAT.

Finally, to test the requirement for this combination of low JNK and JAK/STAT to promote normal DR enhancer behavior in the context of a wound, we investigated the role of each following ablation by DC^{hepCA}. As noted, heterogenous levels of JNK activity are observed during regeneration (Fig 7A-A'''). The inhibition of JAK/STAT signaling via expression of *Stat92E^{RNAi}* does not affect ROS production (S6D' Fig) or JNK levels (Fig 7B-B'''), but does prevent the spread of DR enhancer activity into the wound periphery where JNK is lower (Fig 7B''-B'''). Restricting the formation of different JNK levels

within the wound by blocking cell death to reduce ROS (S6D Fig) and thus limit feedforward JNK signaling results in *DR^{WNT}-GFP* expression becoming spatially restricted to where JNK is initially expressed and not in the wound periphery (Fig 7C''-C'''). Restricting the formation of different JNK levels via *mir(RHG)* and JAK/STAT signaling via *Stat92E^{RNAi}* together phenocopies this result (Fig 7D). Thus, within an injury the activation of DR enhancers requires either the high levels of JNK found at the center of the wound, or the combination of lower JNK and JAK/STAT in the periphery.

Together, these data suggest a model in which distinct thresholds of JNK activity exist to regulate regenerative gene expression (Fig 7E-H'). At high levels, JNK alone is sufficient to activate DR enhancers in the center of the wound (Fig 7E-E'). This high JNK also leads to JAK/STAT signaling, which over time becomes switched off by JNK autonomously, but activated non-autonomously in the wound periphery where JNK is lower (Fig 7F-F'). The combination of lower JNK and JAK/STAT in these cells can activate DR enhancers, leading to their induction outside of the higher JNK domain (Fig 7F-F'). Here the level of JNK is below the threshold necessary to activate DR enhancers by itself, and therefore when JAK/STAT is removed, DR enhancers are no longer induced in the wound periphery (Fig 7G-G'). Similarly, when cell death is blocked by mir(RHG), limiting the production of ROS necessary for JNK to spread beyond the center of the wound, DR enhancer activity is similarly restricted to the high JNK domain (Fig H-H'). Together this dynamic ensures that DR enhancers are activated appropriate to the extent of injury, dictated by the level of JNK activity produced, while the requirement for JAK/STAT results in their activity spreading beyond the initial site of injury across a developing wound. Since DR enhancers potentially regulate multiple genes as part of the regeneration program (16), these data demonstrate a mechanism that allows discrete threshold levels of JNK signaling to not only control the proper magnitude, timing and spatial extent of gene activation in response to injury, but also distinguishes between the activation of targets required for regeneration versus those necessary for normal development.

Discussion

Our work previously identified and characterized DRMS enhancers; regulatory elements within the *Drosophila* genome that respond to damage by driving the expression of numerous genes required for regeneration, which can become shut off with developmental maturity to limit tissue repair with organismal age (8, 16). These enhancers are activated by JNK signaling via a damage-responsive (DR) region, although how this activation is limited specifically to injury and does not occur in other JNK-dependent contexts, such as embryogenesis or pupariation (24-27) has not been explored. Similarly, it is unclear how the magnitude of an injury is translated from the activity of a single pathway (JNK) into the spatially dynamic expression of different downstream target genes necessary for proper regeneration. Our current work has addressed both of these issues. Firstly, by isolating JNK signaling from the downstream events of apoptotic signaling, we have shown that DR enhancers can be activated independent of cell death, requiring only JNK and its immediate targets. We also found that one of these immediate targets, JAK/STAT, is an additional direct input into enhancer activity alongside JNK. By testing each input separately, we have demonstrated that a high enough level of JNK is sufficient to initially activate DR enhancers, while JAK/STAT is required to amplify and expand this activity into more proximal regions of the wound where JNK alone is insufficient. Below this threshold only certain JNK targets, such as those that occur during development like *puc,* are expressed. Within a wound, apoptosis promotes P38 and high JNK activity via ROS and other mechanisms in surrounding cells (22, 62). This level of JNK activates DR enhancers, and thus their targets like *wg* and *Mmp1*, alongside promoting a senescence-like phenotype associated with a temporary pause of proliferation (47). JNK activity also promotes JAK/STAT signaling via the expression of *upd* ligands (22, 29, 31, 46, 49, 50), which in an early wound initially acts in an autocrine fashion, but subsequently becomes paracrine, occurring in the wound periphery where JNK levels are too low to activate DR enhancers alone (47). In these outer regions, JAK/STAT signaling together with JNK allows DR enhancers and their targets to be expressed, thus extending and sustaining the activation of the regeneration program

outside the initial area of JNK activity induced by damage. Our data show that when JAK/STAT signaling is inhibited, or when JNK is prevented from spreading outside of its initial domain by blocking cell death signaling that normally allows ROS-dependent feedforward JNK signaling, this peripheral enhancer activation no longer occurs, thus restricting the regeneration program to the immediate wound area and impairing the overall ability to recover. As such, DR enhancers are necessary to both activate regenerative gene expression downstream of JNK, and to translate heterogenous levels of JNK into spatially and temporally dynamic expression patterns of different factors required for regeneration.

DRMS enhancers as a mechanism to spatially regulate regenerative gene expression

Enhancers that appear to be primarily or wholly dedicated to regeneration have been identified in diverse organisms and tissue contexts (5, 6, 63). For example, in highly regenerative Zebrafish, such enhancers at the *leptin B* and *ctgfa* genes have been characterized in heart and fin regeneration (9, 64), while numerous damage-responsive loci have been identified across the genome related to both tissues (65, 66). Evidence suggests that such regulatory elements function in numerous other models of injury, potentially even in humans (67, 68). The existence of these enhancers is perhaps unsurprising given the need for expression patterns that are unique to regeneration, such as those that occur during wound healing, or that connect the healing phase to the subsequent re-engagement of developmental expression patterns. Indeed, genome-wide assays have demonstrated the existence of such unique transcriptional and epigenetic profiles in case of axolotl, Xenopus, mouse and *Drosophila* regeneration (48, 69-73). Yet, our work in imaginal discs suggests that regeneration enhancers go beyond simply activating reparative gene expression but also play an important role in producing heterogeneity in the regenerative response. Having the major players of a regeneration program activated primarily by a

single pathway (JNK) permits immediate and coordinated initiation of reparative gene expression. However, a mechanism is also required to ensure that different levels of such a signal caused by distance from injury, or variations in its activation due to tissue identity (74), are properly interpreted to generate the diversity of gene expression needed for regeneration. The DR enhancers we have characterized enable this by translating the extent of JNK signaling and the different levels that accrue around a wound into the appropriate activation of different downstream target genes needed for recovery. Indeed, comparing discs in which the entire wing pouch is undergoing ablation versus only the distal pouch (8, 16), or in clonal patches of varying size that are induced to die in the wing and other different imaginal discs (8) supports the idea that DR enhancers promote spatial diversity in gene expression based on the degree of JNK activity produced. Such diversity has been demonstrated by single cell sequencing in ablated wing discs (48, 73), showing that cell populations with discrete cellular identities are formed following injury and change over time. Wound striation is generated by the formation of a central JNK expressing population, which gains a senescence-like phenotype, downregulating markers for proliferation, expressing factors to limit differentiation like *Ets21C* and paracrine signaling factors like *wg* and the *upds* ligands (47, 48, 73). Meanwhile, cells of the periphery receive these signals, have high levels of JAK/STAT activation and express factos that support survival and proliferation, (47, 48, 73). The establishment of regions with specific transcriptional identities that properly coordinate growth and repatterning are key to proper regeneration (47), while DR enhancers contribute to the formation of this regionality in response to injury.

Signaling factors that activate and regulate DR enhancers are potentially conserved

JNK and JAK/STAT signaling are both essential for proper regeneration in *Drosophila*, with each playing complex roles in proliferation, cell death or survival, and cellular identity, among others (42, 44).

While JAK/STAT has been well established as an important regulator of regeneration in *Drosophila* (29, 31, 44-47) many of its established functions depend on prior JNK expression. Thus, it is possible that many such processes involve DR enhancers, while differences in threshold interpretations could dictate whether a gene is expressed in different regional subsets of cells within the wound following damage, or in the wound periphery. JNK signaling is associated with the activity of regeneration enhancers in most instances where they have been identified – indeed, AP-1 binding sites are overrepresented or functionally required in DR enhancers found in organisms with highly contrasting abilities to regenerate, such as zebrafish and mammals (9, 65, 75-77), and in diverse tissues, from imaginal discs to Schwann cells (8, 16, 18, 78), suggesting that JNK might be a highly conserved input into these enhancers (6). Currently, JAK/STAT has yet to be implicated in the activation of DR enhancers in other organisms, but is known to be necessary for proper regeneration in many cases, including those where DR enhancer have been identified. For example, caudal fin regeneration in Zebrafish is impaired upon the loss of *Stat3* due to aberrations in macrophage recruitment and other mechanisms (79). Thus, it will be important to test whether a similar DR enhancer regulatory role for JAK/STAT exists in other organisms. It is also possible that other signals act on such enhancers to refine their expression, as JAK/STAT does. Additional screening by our lab has yet to identify such a signal in *Drosophila*, although the multitiered interactions that exist in the regulation of regenerative gene expression may make their identification challenging (80). Regardless of the involvement of other pathways, the identification of JAK/STAT as a novel input into DR enhancers further defines the regulatory signature of regions that promote regeneration, which may aid in their identification and that of gene regulatory networks responsible (GRNs) for regeneration in *Drosophila* and other species.

A notable example in which a hierarchical GRN required for regeneration has been mapped is in the acoel worm, in which Early growth response (Egr) acts as a master regulator to active numerous genes in response to amputation injury (43). Egr acts as a pioneer factor to directly regulate the activity of multiple downstream targets by modifying epigenetic accessibility, in addition to acting as a traditional

transcription factor for certain targets. Here again, the motif for AP-1 (Jun/Fos) is highly enriched in damage-responsive regions regulated by Egr (43). These top-tier changes subsequently induce expression of other genes within the GRN, leading to the complex transcriptional patterns in different cell types of the epidermis, muscle, neurons and stem cells necessary for regeneration. Since DRs enhancers in imaginal discs are also epigenetically regulated, becoming more accessible upon injury (8, 16), it is possible that a similar regulatory situation might exist in which AP-1 not only acts as a transcription factor but also as a pioneer factor, which has been shown to be the case in mammalian contexts (81-83), although to our knowledge this has yet to be demonstrated in *Drosophila*. The best characterized pioneer factors in *Drosophila* are encoded by *grainy head* (*grh*) and *zelda* (*zld*), the latter of which has recently been shown to be important for maintaining cell fate identity in regenerating wing discs (84). Therefore, testing the importance of these factors may reveal more about how DR enhancers are regulated to control the regeneration program in *Drosophila*.

Establishing a JNK threshold necessary for DR enhancer activation.

JNK signaling has been studied extensively for its role in regeneration, and it is often assumed that the level or duration of JNK signaling leads to distinct signaling outcomes (42, 62). For example, low or transient levels of JNK leading to cell proliferation and survival, while higher or sustained JNK leads to cell death (61). The autocrine versus paracrine modality of JNK signaling likely contributes to these different outcomes (42), while the distinct function of JNK receptors might also play an important role. Recently it was shown that the two identified JNK pathway receptors Wengen (Wgn) and Grindlewald (Grnd) are responsive to different inputs following injury, with Grnd activated by the ligand Egr leading to high levels of JNK activity and cell death, and Wgn activated by ROS to promote cell survival and

proliferation via P38 and potentially lower levels of JNK (37). Thus, both the modality of JNK signaling and use of different JNK receptors may be involved in establishing these opposing outcomes.

Our work provides evidence that the discrete level of JNK activity in the disc is a vital property that dictates whether downstream targets are expressed. One aspect that remains to be explored is how JAK/STAT becomes selectively induced at high levels of JNK, thus permitting the activation of specific targets such as *wg* and *Mmp1* in areas where JNK alone is insufficient. It has been shown that P38 is activated alongside JNK in regenerating cells, which together lead to *upd* expression and thus JAK/STAT activity (22). It is also possible that elements of the JAK/STAT pathway are themselves regulated by DR enhancers, and indeed our previous work identified damage-responsive regions adjacent to two of the *upd* ligand genes of JAK/STAT pathway (16). This would infer the existence of an autoregulatory loop of JAK/STAT signaling, similar to the feedforward expression of the JAK/STAT receptor *Dome* that occurs during embryogenesis (85).

Whatever molecular mechanism exists that allows JNK to activate JAK/STAT, and subsequently DR enhancers, much of our understanding of how these regulatory elements might behave to trigger regenerative gene expression come from the examples we have characterized at the WNT and *Mmp1* loci. It is possible that other DR enhancers we have identified (16) respond differently to the same level of JNK activity (have a different threshold requirement), or rely on additional signaling events other than JAK/STAT. Experiments to examine the genome-wide epigenetic and transcriptomic changes that occur in response to damage when signaling pathways such as JNK, JAK/STAT or other candidate pathways are altered, as have been done in other studies (43), would help to establish the proportion of DR enhancers that act in the way we have described, responding to particular signaling threshold levels or requiring alternative signaling pathways to contribute to imaginal disc regeneration.

Despite being a comparatively recent discovery, the existence of DR regulatory elements has already led to unique insights into the identity, initiation and behavior of genes that promote regeneration. As our work here shows, these enhancers are activated specifically by injury and can interpret a single

damage signal into the spatially dynamic patterns of gene expression required for proper regeneration, while automatically shutting off once regeneration is complete. As such, they are an ideal regulatory vehicle with which to manipulate repair processes, an idea that has already led to the development of methods to direct the expression of both endogenous genes and exogenous factors to improve regeneration and tissue function in various organisms (8, 9), including adult mammals (10). Thus, it will be essential to further advance our understanding of this regulatory mechanism in future.

Materials and Methods

Drosophila stocks

Flies were cultured in conventional dextrose fly media at 25ºC with 12h light–dark cycles. Genotypes for each figure panel are listed in the Supplementary Genotypes file. Fly lines used as ablation stocks are as follows: hs-FLP; hs-p65; salm-LexADBD, DVE>>GAL4 (DC^{NA}), hs-p65/CyO; salm-LexADBD, DVE>>GAL4/ TM6B, Tb (DC^{hepCA})(16). Ablation stocks used for RNA-seq were previously outlined in (Harris et al. 2020). DR/DRMS reporters were previously described in (8, 16). The following stocks were obtained from Bloomington Drosophila Stock Center: AP-1-RFP (BL#59011), puc-lacZ (BL#11173), 10XSTAT-dGFP (BL#26200, BL#26199), 10XSTAT-GFP (BL#26197), UAS-Stat92E^{RNAi} (BL#33637), hh-GAL4 (BL#600186), Pnr-GAL4 (BL#3039), rn-GAL4 (BL#7405), Ptc-GAL4 (BL#44612), UAS-Hep^{CA} (BL#6406) UAS-Hep^{WT} (BL#3908), salm[GMR85E08]-GAL4 (BL#46804), mol-lacZ (BL#12173). UAS-mir(RHG) was a gift from the Iswar Hariharan at UC Berkeley (Siegrist et al. 2010), UAS-hop48a (UAS-hop) and UAS-hop^{ORF} were gifts from the Erika Bach at NYU. Stocks generated for this work: DR^{WNT}ΔStat92E, DR^{WNT}-RFP, DR^{WNT}-GFP (III). Detailed maps and cloning procedures available on request. Transgenic services were provided by BestGene (Chino Hills, CA)

Ablation experiments

DUAL Control ablation. DUAL Control experiments were performed essentially as described in (16). Briefly, experimental crosses were cultured at 25°C and density controlled at 50 larvae per vial. Larvae were heat shocked on day 3.5 (84 h after egg deposition [AED]) or day 4.5 (108 h AED) of development by placing vials in a 37°C water bath for 45 min, followed by a return to 25°C. Larvae were allowed to recover for 18 h before being dissected, fixed and immunolabeled, unless otherwise indicated. *UAS-y^{RNAi}* were used as control lines for RNAi-based experiments.

GAL4/UAS ablation. GAL4/UAS-based ablation experiments were performed essentially as described in (16). Briefly, larvae bearing rn-*GAL4, $GAL80^{ts}$, UAS-egr* were cultured at 18°C and density controlled

at 50 larvae per vial. Larvae were upshifted on day 7 (168 hr AED) or day 9 of development (216 hr AED) for 40 hr at 30°C and dissected into Trizol immediately and prepared for RNA-seq.

Inducing JNK at different levels

Flies of genotype *UAS-hep^{WT}, UAS-mi(RHG), salm[GMR85E08]-GAL4* were used for JNK^{Low} and JNK^{Med} conditions. Crosses were density controlled at 50 larvae per vial and kept at either 22°C (JNK^{Low}) or 30°C (JNK^{Med}) until mid L3 (120 h and 88 h AED) respectively before being dissected, fixed, and stained. Flies of genotype *UAS-hep^{CA}, UAS-mi(RHG), GAL80^{ts}, salm[GMR85E08]-GAL4* were used for the JNK^{High} condition. Crosses were density controlled at 50 larvae per vial and kept at 18°C until day 6 (144 h AED) when they were transferred to 30°C for 20 hours before being dissected, fixed, and stained.

Immunohistochemistry

Larvae were dissected in 1 x PBS followed by a 20 min fix in 4 % paraformaldehyde in PBS (PFA). After 3 washes in 0.1 % PBST (1 x PBS + 0.1 % Triton-X), larvae were washed in 0.3% PBST and then blocked in 0.1 % PBST with 5 % normal goat serum (NGS) for 30 min. Primary staining was done overnight at 4°C, and secondary staining was done for 4 hr at room temperature. The following primary antibodies were obtained from the Developmental Studies Hybridoma Bank: mouse anti-Nubbin (1:25), mouse anti-Wg (1:100), mouse anti-Mmp1 C-terminus (1:100), mouse anti-Mmp1 catalytic domain (1:100), mouse anti-LacZ (1:100), rat anti-Ci (1:3) and rat anti-DE-cadherin (1:100). Antibodies obtained from Cell Signaling Technologies: Rabbit anti-Dcp-1 (1:1000), mouse anti-PH3 (1:500). Secondary antibodies anti-rabbit 647, and anti-mouse 555 and anti-rat 555 were obtained from Invitrogen and used at a 1:500 dilution. DAPI (1:1000) was used as a counterstain. Images were obtained on a Zeiss AxioImager M2 with ApoTome. For each experiment at least 15 discs were analyzed prior to choosing a representative image. Images were processed using Affinity Photo and Affinity Designer. All images are set to the scale bar being 50 μm in length unless otherwise stated in the figure legend.

DHE staining

Dihydroethidium (DHE) labeling was performed by incubating freshly dissected wing imaginal discs in Schneider's Media with 1 µl of 10 mM DHE reconstituted in 1 ml DMSO (for a working concentration of 10 µm DHE) for 10 min, followed by three 5 min washes in PBS, fixed in 4% PFA for 8 mins, a further 1 min wash in PBS, followed by mounting and immediate imaging.

Regeneration scoring and wing measurements

Wings of adult flies from heat shocked larvae were scored and measured after genotype blinding by another researcher. Scoring was performed on anesthetized adults by binning into a regeneration scoring category (16, 86). Wing measurements were performed by removing wings, mounting in Permount solution (Fisher Scientific) and imaged using a Zeiss Discovery V8 microscope. Wing area was measured using the Fiji software. Male and female adults were measured separately to account for sex differences in wing size using a reproducible measuring protocol that excludes the variable hinge region of the wing (details of measuring protocol available on request). Statistics were performed using GraphPad Prism 10.0.

Quantification, Fluorescence Measurement and Statistical Analysis

Adult wings, mean fluorescence intensity, and cell counts were measured using Fiji. GraphPad Prism 10.0 was used for statistical analysis and graphical representation. Graphs depict the mean of each treatment, while error bars represent the standard deviation. The mean fluorescence intensity (MFI) was quantified in Fiji. In each experiment, MFI of the wing pouch was normalized to the MFI of the non-fluorescent notum. For measurement of STAT in the AP-1 domain (Fig 3H) the area of the AP-1 expression domain was selected and the MFI of 10XSTAT-dGFP in this domain was measured and normalized. For measurement of PH3 cell number (Fig 3K), cells were counted using the ImageJ cell

counter plug-in. The wound center and periphery areas were selected by outlining the areas of high and low JNK expression using the AP-1 reporter, and the cells in each area counted. For all quantifications the mean and standard deviation for each normalized treatment was calculated and used for statistical analysis. The sample size and p values for all statistical analyses are indicated in the figure legends. Statistical significance was evaluated in Prism 10.0 using statistical test stated. Figures were made using Biorender.com.

qRT-PCR analysis

Total RNA was extracted from 15 wing discs per sample using the TRIzol reagent (Thermo Fisher Scientific), and cDNA libraries were prepared from total RNA using the AzuraQuant cDNA synthesis kit (Azuragenomics) according to manufacturers instructions. qRT-PCR was performed using AzuraQuant Green 1-step qPCR Mix LoRox (Azuragenomics) on a ThermoFisher Quant Studio3. Data were analyzed using the ΔΔCt method and normalized to the housekeeping gene actin5C. Primer sequences used for PCR: *Act5C* Fwd GGCGCAGAGCAAGCGTGGTA, Rvse GGGTGCCACACGCAGCTCAT; *DsRed* Fwd CACTACCTGGTGGAGTTCAAG, Rvse GATGGTGTAGTCCTCGTTGTG.

RNA-seq

Library prep and RNA-Sequencing (RNA-Seq) was performed by the QB3 Genomics Facility at UC Berkeley from total RNA of ~100 discs per sample using polyT adapters and sequenced on the Illumina Miseq platform.

Data processing. The RNA-Sequencing (RNA-Seq) data was processed using a pipeline that included quality control, trimming, read alignment, and gene expression quantification. Adapters and low-quality reads were trimmed using Trim Galore (bioinformatics.babraham.ac.uk/projects/trim_galore) using the Phred quality score of 20. We visualized quality of the raw and trimmed reads using FastQC and MultiQC (87). Trimmed reads were aligned to the *Drosophila melanogaster* reference genome obtained from FlyBase (Flybase.org; version r6.57) using HISAT2 (88). The resulting BAM files were sorted, and

coverage statistics were calculated using SAMtools (89). Finally, gene-level read counts were obtained using featureCounts based on the *Drosophila melanogaster* annotation (version r6.57), also obtained from FlyBase (90).

Differential expression. Differential gene expression analysis was performed using the limma package in R (91) with the voom transformation (92) applied to account for the mean-variance relationship in RNA-seq data. After transforming the read counts into LOG_2-counts per million (LOG_2-CPM), a linear model was fitted to the data to estimate the differential expression between early and late L3 stages in damaged and undamaged conditions. Empirical Bayes moderation was applied to the standard errors to improve accuracy, and p-values were adjusted for multiple testing using the Benjamini-Hochberg method. Genes with an adjusted p-value less than or equal to 0.05 and an absolute LOG_2 fold change (LOG_2FC) greater than or equal to 2 were considered differentially expressed.

Gene enrichment analysis. A gene ontology (GO) enrichment analysis was performed using the clusterProfiler package in R (93) to identify the biological functions associated with the differentially expressed genes. The differentially expressed genes identified by the limma-voom analysis were used as input for GO enrichment analysis. Separate analyses were conducted for up-regulated and down-regulated genes between damaged and undamaged conditions in the early and late L3 stages. GO terms were considered significantly enriched if the adjusted p-value was less than or equal to 0.05.

Transcription factor binding site analysis

The coordinates for regions classed as DR peaks (LOG_2FC >0.5 and p adj <0.1) in either early or late L3 discs identified in Harris et al. 2020 were converted from dm3 to the current dm6 version r6.59 using the coordinates converter tool on Flybase (flybase.org/convert/coordinates), and DNA sequences for each peak were extracted using the Extract Genomic DNA tool on Galaxy (usegalaxy.org) in FASTA format. The same process was used to obtain DNA sequences of static peaks, those that do not

change between damaged and undamaged conditions (LOG_2FC <0.5), which were used as the background sequences for TF enrichment analysis. The TF enrichment was performed using the AME tool on Meme Suite (meme-suite.org, (94) with default options, assaying for motifs in the Fly Factor survey database. Identification of Stat92E and AP-1 binding sites in DR regions was performed using the FIMO tool on Meme Suite with default settings and a match p-value of p<0.001 (meme-suite.org, (95)).

Data and reagent availability

Stocks are available upon request and details of stocks and reagents used in this study are available in the materials and methods. The authors affirm that all data necessary for confirming the conclusions of the article are present within the article, figures, and tables. Raw data fastq files are available on SRA Bioproject PRJNA1179511. The code for RNA-seq analysis is available here: https://github.com/mariahlee/Regeneration-in-Drosophila-melanogaster

Acknowledgements

The authors would like to thank Dr. Iswar Hariharan and Dr Erika Bach for their generous gift of stocks and reagents. We thank the current members of the Harris lab for useful input and feedback. We thank the Bloomington Drosophila Stock Center and Developmental Studies Hybridoma Bank for stocks and reagents.

References

1. Sanchez Alvarado A, Tsonis PA. Bridging the regeneration gap: genetic insights from diverse animal models. Nat Rev Genet. 2006;7(11):873-84.
2. Li Q, Yang H, Zhong TP. Regeneration across metazoan phylogeny: lessons from model organisms. J Genet Genomics. 2015;42(2):57-70.
3. Tanaka EM, Reddien PW. The cellular basis for animal regeneration. Dev Cell. 2011;21(1):172-85.
4. Tanaka EM. The Molecular and Cellular Choreography of Appendage Regeneration. Cell. 2016;165(7):1598-608.
5. Rodriguez AM, Kang J. Regeneration enhancers: Starting a journey to unravel regulatory events in tissue regeneration. Semin Cell Dev Biol. 2020;97:47-54.
6. Harris RE. Regeneration enhancers: a field in development. Am J Physiol Cell Physiol. 2022;323(5):C1548-C54.
7. Suzuki N, Ochi H. Regeneration enhancers: A clue to reactivation of developmental genes. Dev Growth Differ. 2020;62(5):343-54.
8. Harris RE, Setiawan L, Saul J, Hariharan IK. Localized epigenetic silencing of a damage-activated WNT enhancer limits regeneration in mature Drosophila imaginal discs. Elife. 2016;5.
9. Kang J, Hu J, Karra R, Dickson AL, Tornini VA, Nachtrab G, et al. Modulation of tissue repair by regeneration enhancer elements. Nature. 2016;532(7598):201-6.
10. Yan R, Cigliola V, Oonk KA, Petrover Z, DeLuca S, Wolfson DW, et al. An enhancer-based gene-therapy strategy for spatiotemporal control of cargoes during tissue repair. Cell Stem Cell. 2023;30(1):96-111 e6.
11. Tripathi BK, Irvine KD. The wing imaginal disc. Genetics. 2022;220(4).
12. Beira JV, Paro R. The legacy of Drosophila imaginal discs. Chromosoma. 2016;125(4):573-92.

13. Worley MI, Setiawan L, Hariharan IK. Regeneration and transdetermination in Drosophila imaginal discs. Annu Rev Genet. 2012;46:289-310.

14. Worley MI, Hariharan IK. Imaginal Disc Regeneration: Something Old, Something New. Cold Spring Harb Perspect Biol. 2022;14(11).

15. Fox DT, Cohen E, Smith-Bolton R. Model systems for regeneration: Drosophila. Development. 2020;147(7).

16. Harris RE, Stinchfield MJ, Nystrom SL, McKay DJ, Hariharan IK. Damage-responsive, maturity-silenced enhancers regulate multiple genes that direct regeneration in Drosophila. Elife. 2020;9.

17. Harris RE. Investigating Tissue Regeneration Using the DUAL Control Genetic Ablation System. Methods Mol Biol. 2023;2599:255-70.

18. Vizcaya-Molina E, Klein CC, Serras F, Mishra RK, Guigo R, Corominas M. Damage-responsive elements in Drosophila regeneration. Genome Res. 2018;28(12):1852-66.

19. Gracia-Latorre E, Perez L, Muzzopappa M, Milan M. A single WNT enhancer drives specification and regeneration of the Drosophila wing. Nat Commun. 2022;13(1):4794.

20. Smith-Bolton RK, Worley MI, Kanda H, Hariharan IK. Regenerative growth in Drosophila imaginal discs is regulated by Wingless and Myc. Dev Cell. 2009;16(6):797-809.

21. Bergantinos C, Corominas M, Serras F. Cell death-induced regeneration in wing imaginal discs requires JNK signalling. Development. 2010;137(7):1169-79.

22. Santabarbara-Ruiz P, Lopez-Santillan M, Martinez-Rodriguez I, Binagui-Casas A, Perez L, Milan M, et al. ROS-Induced JNK and p38 Signaling Is Required for Unpaired Cytokine Activation during Drosophila Regeneration. PLoS Genet. 2015;11(10):e1005595.

23. Mattila J, Omelyanchuk L, Kyttala S, Turunen H, Nokkala S. Role of Jun N-terminal Kinase (JNK) signaling in the wound healing and regeneration of a Drosophila melanogaster wing imaginal disc. Int J Dev Biol. 2005;49(4):391-9.

24. Zeitlinger J, Bohmann D. Thorax closure in Drosophila: involvement of Fos and the JNK pathway. Development. 1999;126(17):3947-56.

25. Agnes F, Suzanne M, Noselli S. The Drosophila JNK pathway controls the morphogenesis of imaginal discs during metamorphosis. Development. 1999;126(23):5453-62.

26. Harden N. Signaling pathways directing the movement and fusion of epithelial sheets: lessons from dorsal closure in Drosophila. Differentiation. 2002;70(4-5):181-203.

27. Kiehart DP, Crawford JM, Aristotelous A, Venakides S, Edwards GS. Cell Sheet Morphogenesis: Dorsal Closure in Drosophila melanogaster as a Model System. Annu Rev Cell Dev Biol. 2017;33:169-202.

28. Uhlirova M, Bohmann D. JNK- and Fos-regulated Mmp1 expression cooperates with Ras to induce invasive tumors in Drosophila. EMBO J. 2006;25(22):5294-304.

29. Katsuyama T, Comoglio F, Seimiya M, Cabuy E, Paro R. During Drosophila disc regeneration, JAK/STAT coordinates cell proliferation with Dilp8-mediated developmental delay. Proc Natl Acad Sci U S A. 2015;112(18):E2327-36.

30. Khan SJ, Abidi SNF, Skinner A, Tian Y, Smith-Bolton RK. The Drosophila Duox maturation factor is a key component of a positive feedback loop that sustains regeneration signaling. PLoS Genet. 2017;13(7):e1006937.

31. La Fortezza M, Schenk M, Cosolo A, Kolybaba A, Grass I, Classen AK. JAK/STAT signalling mediates cell survival in response to tissue stress. Development. 2016;143(16):2907-19.

32. Fogarty CE, Bergmann A. Killers creating new life: caspases drive apoptosis-induced proliferation in tissue repair and disease. Cell Death Differ. 2017;24(8):1390-400.

33. Morata G, Shlevkov E, Perez-Garijo A. Mitogenic signaling from apoptotic cells in Drosophila. Dev Growth Differ. 2011;53(2):168-76.

34. Fogarty CE, Diwanji N, Lindblad JL, Tare M, Amcheslavsky A, Makhijani K, et al. Extracellular Reactive Oxygen Species Drive Apoptosis-Induced Proliferation via Drosophila Macrophages. Curr Biol. 2016;26(5):575-84.

35. Amcheslavsky A, Wang S, Fogarty CE, Lindblad JL, Fan Y, Bergmann A. Plasma Membrane Localization of Apoptotic Caspases for Non-apoptotic Functions. Dev Cell. 2018;45(4):450-64 e3.

36. Pinal N, Martín M, Medina I, Morata G. Short-term activation of the Jun N-terminal kinase pathway in apoptosis-deficient cells of Drosophila induces tumorigenesis. Nature Communications. 2018;9(1).

37. Esteban-Collado J, Fernandez-Manas M, Fernandez-Moreno M, Maeso I, Corominas M, Serras F. Reactive oxygen species activate the Drosophila TNF receptor Wengen for damage-induced regeneration. EMBO J. 2024;43(17):3604-26.

38. Diwanji N, Bergmann A. The beneficial role of extracellular reactive oxygen species in apoptosis-induced compensatory proliferation. Fly (Austin). 2017;11(1):46-52.

39. Siegrist SE, Haque NS, Chen CH, Hay BA, Hariharan IK. Inactivation of both Foxo and reaper promotes long-term adult neurogenesis in Drosophila. Curr Biol. 2010;20(7):643-8.

40. Su TT. Non-autonomous consequences of cell death and other perks of being metazoan. AIMS Genet. 2015;2(1):54-69.

41. Martín FA, Peréz-Garijo A, Morata G. Apoptosis in Drosophila: Compensatory proliferation and undead cells. International Journal of Developmental Biology. 2009;53(8-10):1341-7.

42. Pinal N, Calleja M, Morata G. Pro-apoptotic and pro-proliferation functions of the JNK pathway of Drosophila: roles in cell competition, tumorigenesis and regeneration. Open Biol. 2019;9(3):180256.

43. Gehrke AR, Neverett E, Luo YJ, Brandt A, Ricci L, Hulett RE, et al. Acoel genome reveals the regulatory landscape of whole-body regeneration. Science. 2019;363(6432).

44. Herrera SC, Bach EA. JAK/STAT signaling in stem cells and regeneration: from Drosophila to vertebrates. Development. 2019;146(2).

45. Verghese S, Su TT. Drosophila Wnt and STAT Define Apoptosis-Resistant Epithelial Cells for Tissue Regeneration after Irradiation. PLoS Biol. 2016;14(9):e1002536.

46. Ahmed-de-Prado S, Diaz-Garcia S, Baonza A. JNK and JAK/STAT signalling are required for inducing loss of cell fate specification during imaginal wing discs regeneration in Drosophila melanogaster. Dev Biol. 2018;441(1):31-41.

47. Jaiswal J, Egert J, Engesser R, Peyroton AA, Nogay L, Weichselberger V, et al. Mutual repression between JNK/AP-1 and JAK/STAT stratifies senescent and proliferative cell behaviors during tissue regeneration. PLoS Biol. 2023;21(5):e3001665.

48. Floc'hlay S, Balaji R, Stankovic D, Christiaens VM, Bravo Gonzalez-Blas C, De Winter S, et al. Shared enhancer gene regulatory networks between wound and oncogenic programs. Elife. 2023;12.

49. Pastor-Pareja JC, Wu M, Xu T. An innate immune response of blood cells to tumors and tissue damage in Drosophila. Dis Model Mech. 2008;1(2-3):144-54; discussion 53.

50. Worley MI, Alexander LA, Hariharan IK. CtBP impedes JNK- and Upd/STAT-driven cell fate misspecifications in regenerating Drosophila imaginal discs. Elife. 2018;7.

51. Wang H, Chen X, He T, Zhou Y, Luo H. Evidence for tissue-specific Jak/STAT target genes in Drosophila optic lobe development. Genetics. 2013;195(4):1291-306.

52. Mukherjee T, Schafer U, Zeidler MP. Identification of Drosophila genes modulating Janus kinase/signal transducer and activator of transcription signal transduction. Genetics. 2006;172(3):1683-97.

53. Flaherty MS, Salis P, Evans CJ, Ekas LA, Marouf A, Zavadil J, et al. chinmo is a functional effector of the JAK/STAT pathway that regulates eye development, tumor formation, and stem cell self-renewal in Drosophila. Dev Cell. 2010;18(4):556-68.

54. Karsten P, Hader S, Zeidler MP. Cloning and expression of Drosophila SOCS36E and its potential regulation by the JAK/STAT pathway. Mech Dev. 2002;117(1-2):343-6.

55. Yan R, Small S, Desplan C, Dearolf CR, Darnell JE, Jr. Identification of a Stat gene that functions in Drosophila development. Cell. 1996;84(3):421-30.

56. Starz-Gaiano M, Melani M, Wang X, Meinhardt H, Montell DJ. Feedback inhibition of Jak/STAT signaling by apontic is required to limit an invasive cell population. Dev Cell. 2008;14(5):726-38.

57. Bach EA, Ekas LA, Ayala-Camargo A, Flaherty MS, Lee H, Perrimon N, et al. GFP reporters detect the activation of the Drosophila JAK/STAT pathway in vivo. Gene Expr Patterns. 2007;7(3):323-31.

58. Chatterjee N, Bohmann D. A versatile PhiC31 based reporter system for measuring AP-1 and Nrf2 signaling in Drosophila and in tissue culture. PLoS One. 2012;7(4):e34063.

59. Martin-Blanco E, Pastor-Pareja JC, Garcia-Bellido A. JNK and decapentaplegic signaling control adhesiveness and cytoskeleton dynamics during thorax closure in Drosophila. Proc Natl Acad Sci U S A. 2000;97(14):7888-93.

60. Duffy JB. GAL4 system in Drosophila: a fly geneticist's Swiss army knife. Genesis. 2002;34(1-2):1-15.

61. Santabarbara-Ruiz P, Esteban-Collado J, Perez L, Viola G, Abril JF, Milan M, et al. Ask1 and Akt act synergistically to promote ROS-dependent regeneration in Drosophila. PLoS Genet. 2019;15(1):e1007926.

62. La Marca JE, Richardson HE. Two-Faced: Roles of JNK Signalling During Tumourigenesis in the Drosophila Model. Front Cell Dev Biol. 2020;8:42.

63. Yang K, Kang J. Tissue Regeneration Enhancer Elements: A Way to Unlock Endogenous Healing Power. Dev Dyn. 2019;248(1):34-42.

64. Pfefferli C, Jazwinska A. The careg element reveals a common regulation of regeneration in the zebrafish myocardium and fin. Nat Commun. 2017;8:15151.

65. Wang W, Hu CK, Zeng A, Alegre D, Hu D, Gotting K, et al. Changes in regeneration-responsive enhancers shape regenerative capacities in vertebrates. Science. 2020;369(6508).

66. Goldman JA, Kuzu G, Lee N, Karasik J, Gemberling M, Foglia MJ, et al. Resolving Heart Regeneration by Replacement Histone Profiling. Dev Cell. 2017;40(4):392-404 e5.

67. Lander JM, Supp DM, He H, Martin LJ, Chen X, Weirauch MT, et al. Analysis of chromatin accessibility in human epidermis identifies putative barrier dysfunction-sensing enhancers. PLoS One. 2017;12(9):e0184500.

68. Suzuki N, Hirano K, Ogino H, Ochi H. Arid3a regulates nephric tubule regeneration via evolutionarily conserved regeneration signal-response enhancers. Elife. 2019;8.

69. Poss KD. Advances in understanding tissue regenerative capacity and mechanisms in animals. Nat Rev Genet. 2010;11(10):710-22.

70. Gerber T, Murawala P, Knapp D, Masselink W, Schuez M, Hermann S, et al. Single-cell analysis uncovers convergence of cell identities during axolotl limb regeneration. Science. 2018;362(6413).

71. Aztekin C, Hiscock TW, Marioni JC, Gurdon JB, Simons BD, Jullien J. Identification of a regeneration-organizing cell in the Xenopus tail. Science. 2019;364(6441):653-8.

72. Storer MA, Mahmud N, Karamboulas K, Borrett MJ, Yuzwa SA, Gont A, et al. Acquisition of a Unique Mesenchymal Precursor-like Blastema State Underlies Successful Adult Mammalian Digit Tip Regeneration. Dev Cell. 2020;52(4):509-24 e9.

73. Worley MI, Everetts NJ, Yasutomi R, Chang RJ, Saretha S, Yosef N, et al. Ets21C sustains a pro-regenerative transcriptional program in blastema cells of Drosophila imaginal discs. Curr Biol. 2022;32(15):3350-64 e6.

74. Martin R, Morata G. Regenerative response of different regions of Drosophila imaginal discs. Int J Dev Biol. 2018;62(6-7-8):507-12.

75. Thompson JD, Ou J, Lee N, Shin K, Cigliola V, Song L, et al. Identification and requirements of enhancers that direct gene expression during zebrafish fin regeneration. Development. 2020;147(14).

76. Guenther CA, Wang Z, Li E, Tran MC, Logan CY, Nusse R, et al. A distinct regulatory region of the Bmp5 locus activates gene expression following adult bone fracture or soft tissue injury. Bone. 2015;77:31-41.

77. Aguilar CA, Pop R, Shcherbina A, Watts A, Matheny RW, Jr., Cacchiarelli D, et al. Transcriptional and Chromatin Dynamics of Muscle Regeneration after Severe Trauma. Stem Cell Reports. 2016;7(5):983-97.

78. Arthur-Farraj PJ, Morgan CC, Adamowicz M, Gomez-Sanchez JA, Fazal SV, Beucher A, et al. Changes in the Coding and Non-coding Transcriptome and DNA Methylome that Define the Schwann Cell Repair Phenotype after Nerve Injury. Cell Rep. 2017;20(11):2719-34.

79. Sobah ML, Liongue C, Ward AC. Contribution of Signal Transducer and Activator of Transcription 3 (STAT3) to Bone Development and Repair. International journal of molecular sciences. 2023;25(1).

80. Ahmed-de-Prado S, Baonza A. Drosophila as a Model System to Study Cell Signaling in Organ Regeneration. Biomed Res Int. 2018;2018:7359267.

81. Bejjani F, Evanno E, Zibara K, Piechaczyk M, Jariel-Encontre I. The AP-1 transcriptional complex: Local switch or remote command? Biochim Biophys Acta Rev Cancer. 2019;1872(1):11-23.

82. Wolf BK, Zhao Y, McCray A, Hawk WH, Deary LT, Sugiarto NW, et al. Cooperation of chromatin remodeling SWI/SNF complex and pioneer factor AP-1 shapes 3D enhancer landscapes. Nat Struct Mol Biol. 2023;30(1):10-21.

83. Martinez-Zamudio RI, Roux PF, de Freitas J, Robinson L, Dore G, Sun B, et al. AP-1 imprints a reversible transcriptional programme of senescent cells. Nat Cell Biol. 2020;22(7):842-55.

84. Bose A, Schuster K, Kodali C, Sonam S, Smith-Bolton R. The pioneer transcription factor Zelda facilitates the exit from regeneration and restoration of patterning in Drosophila. bioRxiv. 2024.

85. Hombria JC, Brown S, Hader S, Zeidler MP. Characterisation of Upd2, a Drosophila JAK/STAT pathway ligand. Dev Biol. 2005;288(2):420-33.

86. Klemm J, Stinchfield MJ, Harris RE. Necrosis-induced apoptosis promotes regeneration in Drosophila wing imaginal discs. Genetics. 2021;219(3).

87. Ewels P, Magnusson M, Lundin S, Kaller M. MultiQC: summarize analysis results for multiple tools and samples in a single report. Bioinformatics. 2016;32(19):3047-8.

88. Kim D, Paggi JM, Park C, Bennett C, Salzberg SL. Graph-based genome alignment and genotyping with HISAT2 and HISAT-genotype. Nat Biotechnol. 2019;37(8):907-15.

89. Li H, Handsaker B, Wysoker A, Fennell T, Ruan J, Homer N, et al. The Sequence Alignment/Map format and SAMtools. Bioinformatics. 2009;25(16):2078-9.

90. Liao Y, Smyth GK, Shi W. featureCounts: an efficient general purpose program for assigning sequence reads to genomic features. Bioinformatics. 2014;30(7):923-30.

91. Smyth GK. limma: Linear Models for Microarray Data. In: Gentleman R, Carey VJ, Huber W, Irizarry RA, Dudoit S, editors. Bioinformatics and Computational Biology Solutions Using R and Bioconductor. New York, NY: Springer New York; 2005. p. 397-420.

92. Law CW, Chen Y, Shi W, Smyth GK. voom: Precision weights unlock linear model analysis tools for RNA-seq read counts. Genome Biol. 2014;15(2):R29.

93. Wu T, Hu E, Xu S, Chen M, Guo P, Dai Z, et al. clusterProfiler 4.0: A universal enrichment tool for interpreting omics data. Innovation (Camb). 2021;2(3):100141.

94. McLeay RC, Bailey TL. Motif Enrichment Analysis: a unified framework and an evaluation on ChIP data. BMC Bioinformatics. 2010;11:165.

95. Grant CE, Bailey TL, Noble WS. FIMO: scanning for occurrences of a given motif. Bioinformatics. 2011;27(7):1017-8.

Figure 1

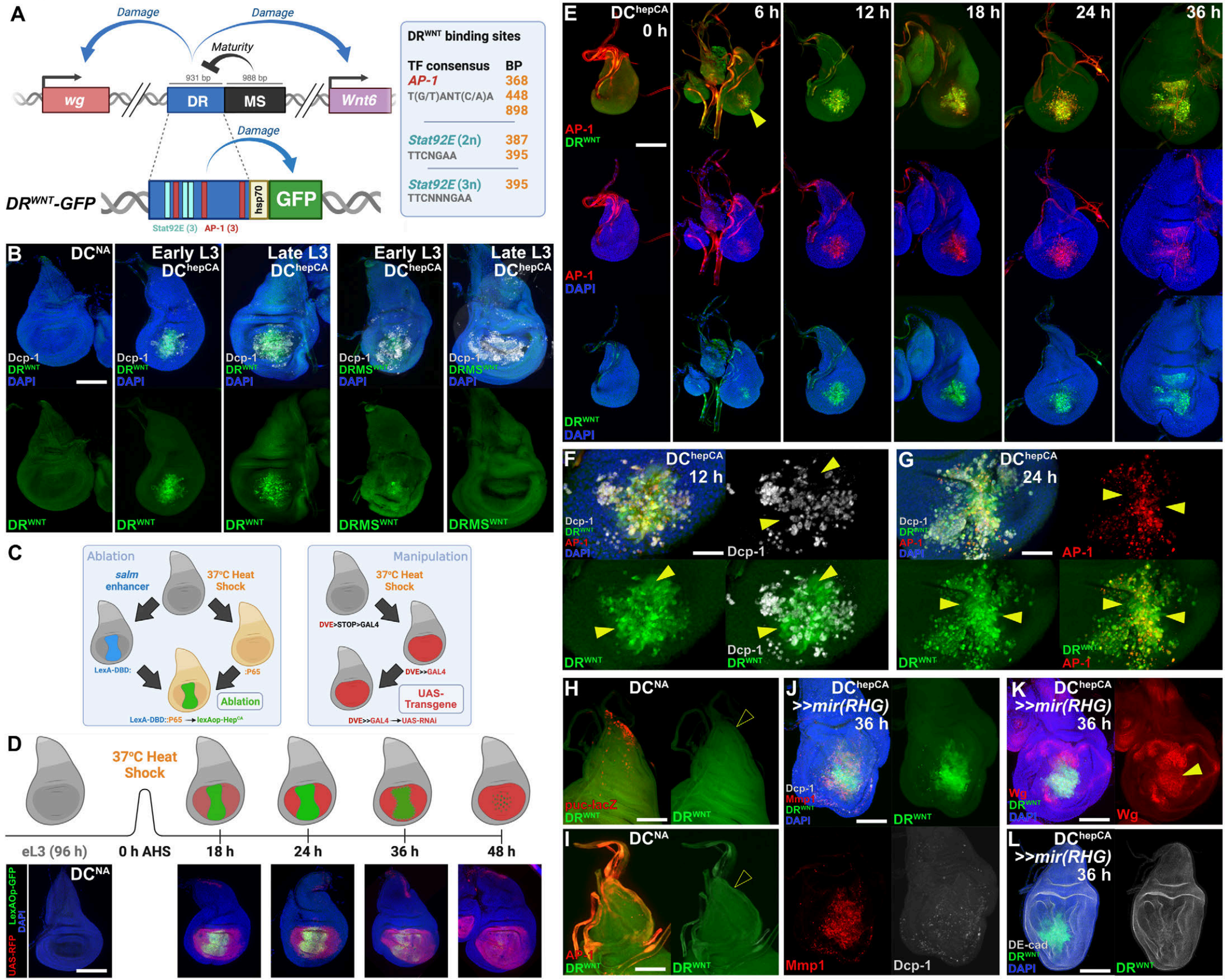
A
Damage
Damage
Maturity
931 bp
988 bp
wg
DR
MS
Wnt6
Damage
DRWNT-GFP
hsp70
GFP
Stat92E (3)
AP-1 (3)
DRWNT binding sites
TF consensus
BP
AP-1
T(G/T)ANT(C/A)A
368
448
898
Stat92E (2n)
TTCNGAA
387
395
Stat92E (3n)
TTCNNNGAA
395
B
DCNA
Early L3
DChepCA
Late L3
DChepCA
Early L3
DChepCA
Late L3
DChepCA
Dcp-1
DRWNT
DAPI
DRMSWNT
C
Ablation
salm enhancer
37°C Heat Shock
LexA-DBD:
:P65
Ablation
LexA-DBD::P65 → lexAop-HepCA
Manipulation
37°C Heat Shock
DVE>STOP>GAL4
DVE>>GAL4
UAS-Transgene
DVE>>GAL4 → UAS-RNAi
D
37°C Heat Shock
eL3 (96 h)
0 h AHS
18 h
24 h
36 h
48 h
DCNA
UAS-RFP
LexAOp-GFP
DAPI
E
DChepCA
0 h
6 h
12 h
18 h
24 h
36 h
AP-1
DRWNT
DAPI
F
DChepCA
12 h
Dcp-1
DRWNT
AP-1
DAPI
G
DChepCA
24 h
Dcp-1
AP-1
DRWNT
H
DCNA
puc-lacZ
DRWNT
I
DCNA
AP-1
J
DChepCA
>>mir(RHG)
36 h
Dcp-1
Mmp1
DRWNT
DAPI
Mmp1
K
DChepCA
>>mir(RHG)
36 h
Wg
DRWNT
DAPI
L
DChepCA
>>mir(RHG)
36 h
DE-cad
DRWNT
DAPI

Figure Legends

Figure 1: DR^{WNT} and the regeneration program can be activated independently of cell death.

(**A**) Schematic of the $DRMS^{WNT}$ regulatory element (top), showing the separable damage-responsive (DR) region that activates *wg* and *Wnt6* expression upon damage, and the maturity-silencing (MS) region that limits DR activity with developmental maturity. The DR^{WNT} reporter (bottom) comprises the DR^{WNT} enhancer DNA, *hsp70* promoter and GFP coding sequence. Schematic shows AP-1 and Stat92E transcription factor binding sites in the DR^{WNT} region, with details shown in table (right). (**B)** Discs bearing the DR^{WNT} or $DRMS^{WNT}$ reporters (green), ablated by DUAL Control (DC^{hepCA}) in early (84 h AED) and late (108 h AED) L3 larvae. Neither reporter is activated in the absence of damage (DC^{NA}). The DR^{WNT} reporter is strongly activated by damage in both early and late L3 discs, while the $DRMS^{WNT}$ reporter is only activated in early L3 discs. (**C)** Schematic of the DC ablation system showing the split LexA-based ablation component (left) and the GAL4-based gene manipulation component (right). Both are induced by a heat shock, upon which ablation is activated in the distal pouch (green) and GAL4 in the whole pouch (red). See main text for details. (**D**) Schematic of the ablation protocol for the DC ablation system (top) with representative discs at each time point (below), showing *lexAop-GFP* expression (green) indicating the ablation domain, and *UAS-RFP* expression (red), showing GAL4 activity. Both reporters are observed at 18 h after heat shock (AHS). Ablation occurs as a pulse of expression that diminishes over time, while GAL4 activity persists throughout regeneration until pupariation. A non-ablating version of DC (DC^{NA}) is used to more clearly show reporter dynamics. (**E)** Time course of discs bearing the DR^{WNT} reporter (green) and AP-1 JNK reporter (red) ablated by DC^{HepCA} and imaged at 0 - 36 h AHS. Both reporters strongly overlap from 6 h (yellow arrowhead) throughout the regeneration period. (**F)** Magnified view of disc as in (E) at 12 h AHS, showing cells with DR^{WNT} activity (green) that lack Dcp-1 (white), indicated by yellow arrowheads. AP-1 reporter (red)

shows JNK activity. **(G)** Magnified view of disc as in (E) at 24 h AHS, showing the DR^{WNT} reporter (green) does not entirely mirror the strength of the AP-1 reporter (red) across the disc, with differences in reporter expression indicated by yellow arrowheads. Dcp-1 (white) shows cells death. **(H-I)** Notum of undamaged discs bearing the DR^{WNT} reporter (green), with developmental JNK expression indicated by the JNK target *puckered* (*puc-lacZ*, red in H) or the AP-1 reporter (*AP-1-RFP*, red in I). The DR^{WNT} reporter is not activated by JNK signaling in the notum. **(J-L)** Discs bearing the DR^{WNT} reporter (green) ablated by DC^{hepCA} and expressing *UAS-mir(RHG)* to block cell death, imaged at 36 h AHS. (J) JNK activity caused by DC^{hepCA} in the absence of cell death activates DR^{WNT}, alongside the JNK target Mmp1 (red). Dcp-1 (white) shows the absence of cell death. (K) JNK activity caused by DC^{hepCA} in the absence of cell death also activates ectopic Wg overlapping the DR^{WNT} reporter (green). (L) JNK activity caused by DC^{hepCA} in the absence of cell death induces overgrowth, indicated by the DE-Cad (white). Scale bars in all panels = 50 μm, except (F-G) = 12.5 μm, (H-J) = 37.5 μm.

Figure 2

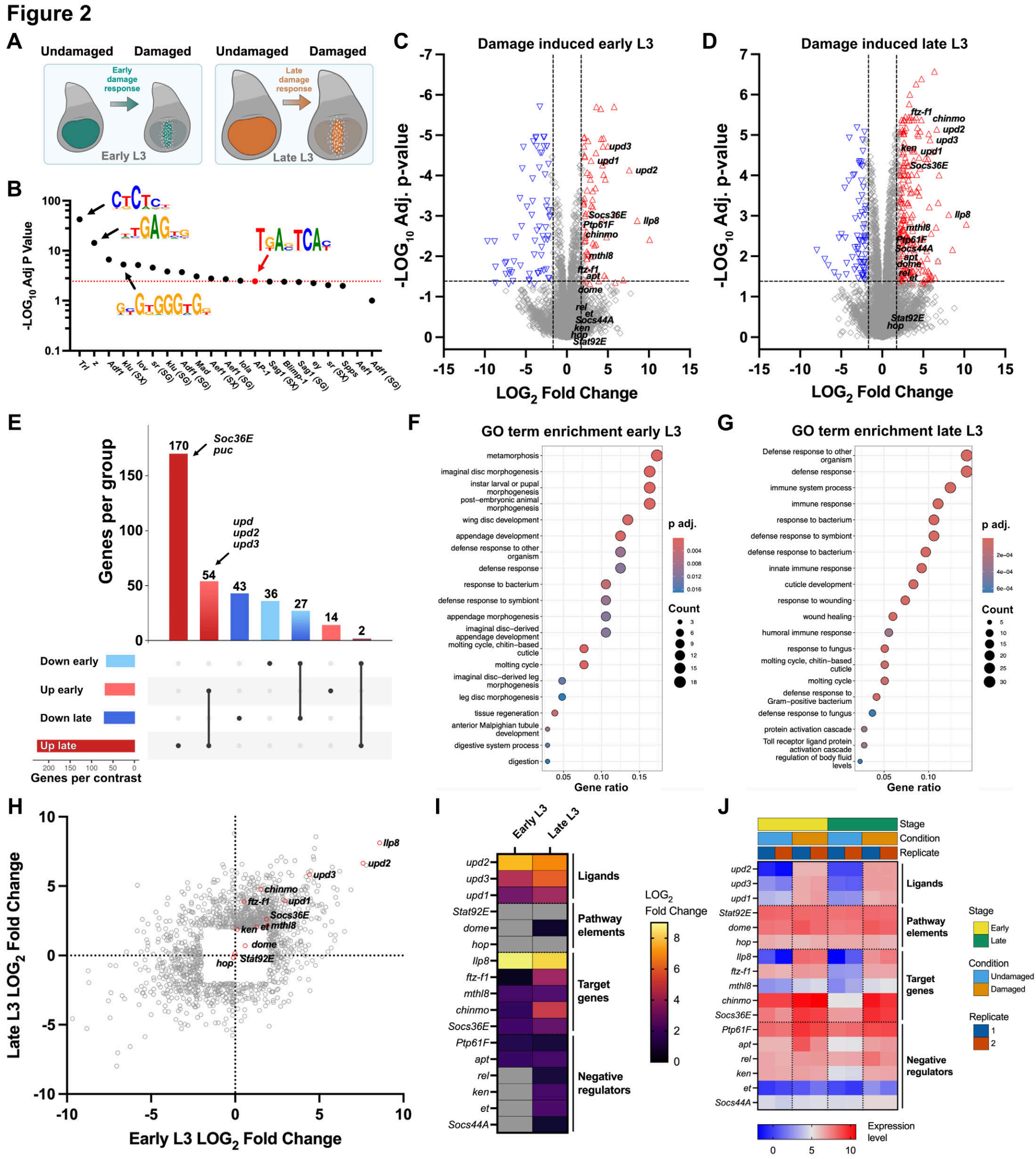
A
Undamaged
Damaged
Undamaged
Damaged
Early damage response
Early L3
Late damage response
Late L3
B
-LOG10 Adj P Value
Trl
z
Adf1
klu (SX)
lov
sr (SG)
klu (SG)
Adf1 (SG)
Mad
Aef1 (SX)
Aef1 (SG)
Iola
AP-1
Sag1 (SX)
Blimp-1
Sag1 (SG)
ey
sr (SX)
Spps
Aef1
Adf1 (SG)
C
Damage induced early L3
-LOG10 Adj. p-value
LOG2 Fold Change
upd3
upd1
upd2
Socs36E
Ptp61F
chinmo
Ilp8
mthl8
ftz-f1
apt
dome
rel
et
Socs44A
ken
hop
Stat92E
D
Damage induced late L3
-LOG10 Adj. p-value
LOG2 Fold Change
ftz-f1
chinmo
upd2
upd3
ken
upd1
Socs36E
Ilp8
mthl8
Ptp61F
Socs44A
apt
dome
rel
et
Stat92E
hop
E
Genes per group
170
Soc36E
puc
54
upd
upd2
upd3
43
36
27
14
2
Down early
Up early
Down late
Up late
Genes per contrast
F
GO term enrichment early L3
metamorphosis
imaginal disc morphogenesis
instar larval or pupal morphogenesis
post-embryonic animal morphogenesis
wing disc development
appendage development
defense response to other organism
defense response
response to bacterium
defense response to symbiont
appendage morphogenesis
imaginal disc-derived appendage development
molting cycle, chitin-based cuticle
molting cycle
imaginal disc-derived leg morphogenesis
leg disc morphogenesis
tissue regeneration
anterior Malpighian tubule development
digestive system process
digestion
Gene ratio
p adj.
Count
G
GO term enrichment late L3
Defense response to other organism
defense response
immune system process
immune response
response to bacterium
defense response to symbiont
defense response to bacterium
innate immune response
cuticle development
response to wounding
wound healing
humoral immune response
response to fungus
molting cycle, chitin-based cuticle
molting cycle
defense response to Gram-positive bacterium
defense response to fungus
protein activation cascade
Toll receptor ligand protein activation cascade
regulation of body fluid levels
Gene ratio
p adj.
Count
H
Late L3 LOG2 Fold Change
Early L3 LOG2 Fold Change
Ilp8
upd2
upd3
chinmo
ftz-f1
upd1
Socs36E
ken
et
mthl8
dome
hop
Stat92E
I
Early L3
Late L3
upd2
upd3
upd1
Stat92E
dome
hop
Ilp8
ftz-f1
mthl8
chinmo
Socs36E
Ptp61F
apt
rel
ken
et
Socs44A
Ligands
Pathway elements
Target genes
Negative regulators
LOG2 Fold Change
J
Stage
Condition
Replicate
Ligands
Pathway elements
Target genes
Negative regulators
Stage
Early
Late
Condition
Undamaged
Damaged
Replicate
Expression level

Figure 2: Differential gene expression and enrichment analysis of regenerating discs identify JAK/STAT as a putative regulator of DR enhancers.

(**A**) Schematic showing conditions used for RNA-seq and ATAC-seq (16) to identify damage-induced changes in early and late L3 discs. Discs were ablated using *rn*^{ts}*>egr* (*rn-GAL4, GAL80ts, UAS-egr*) for 40 hours after culture at 18°C for 168 h (early) or 216 h (late) AED. Discs were isolated and processed for sequencing immediately after ablation. (**B**) Analysis of motif enrichment (AME) performed on DR regions identified in early L3 discs by ATAC-seq. 222 DR regions were analyzed with 7456 static peaks as control sequences. TF identified include chromatin regulators *Trl*, *z* and *klu*, and the JNK pathway TF, *kay/jra* (AP-1). Detected consensus site sequences are labelled. (**C-D**) Volcano plots of differentially expressed genes induced by damage identified by RNA-seq. LOG_2 fold change (LOG_2FC) vs. significance (-LOG_{10} adjusted p-value) of genes expressed in (C) early and (D) late L3 stages between damaged vs. undamaged conditions. Genes related to the JAK/STAT pathway are labelled. (**E**) Upset plot showing the intersections of genes that are upregulated or downregulated in early and late L3 stages under damaged and undamaged conditions, where horizontal bars represent the total number of genes per group, and vertical bars display the numbers of genes that overlap between the groups. The *upd* ligands are upregulated in both early and late L3 damaged discs, while the well characterized negative regulators of JNK and JAK/STAT signaling, *puc* and *Socs36E*, are upregulated in late L3 discs (labelled). (**F-G**) Gene ontology analysis of factors differentially expressed between damaged and undamaged in early (F) and late (G) L3 discs. The x-axis shows the ratio of genes in a category to all differentially expressed genes (gene ratio), dot size indicates the number of genes in each enriched category, heatmap indicates adjusted p-value. (**H**) Comparison of the fold change (LOG_2FC) of all genes between damaged and undamaged in early L3 versus late L3, plotting differentially expressed genes in grey and JAK/STAT pathway genes in red with labels. (**I**) Heatmap

comparing damage-induced fold change (LOG_2FC) of genes related to JAK/STAT signaling, including the ligands, pathway transducers, selected target genes and known negative regulators in early L3 versus late L3 discs. Gray cells indicate p-value is not significant ($p>0.05$). (**J**) Heatmap of the expression levels of JAK/STAT pathway genes across each stage (early vs late), damage condition (undamaged versus damaged) and replicate (first or second biological repeat), with red representing higher expression and blue representing lower expression.

Figure 3

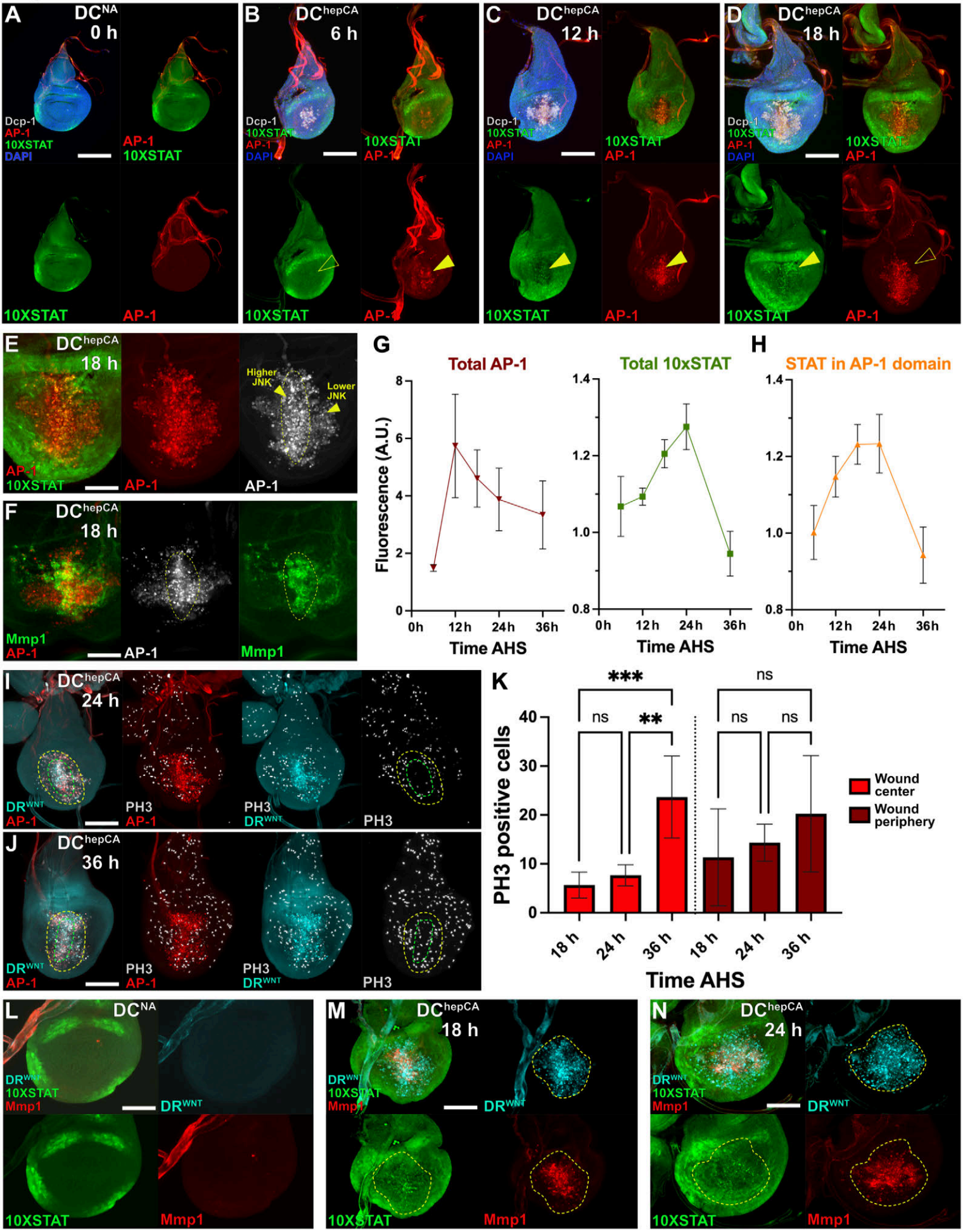
A
DCNA
0 h
Dcp-1
AP-1
10XSTAT
DAPI
AP-1
10XSTAT
10XSTAT
AP-1
B
DChepCA
6 h
Dcp-1
10XSTAT
AP-1
DAPI
10XSTAT
AP-1
10XSTAT
AP-1
C
DChepCA
12 h
Dcp-1
10XSTAT
AP-1
DAPI
10XSTAT
AP-1
10XSTAT
AP-1
D
DChepCA
18 h
Dcp-1
10XSTAT
AP-1
DAPI
10XSTAT
AP-1
10XSTAT
AP-1
E
DChepCA
18 h
Higher JNK
Lower JNK
AP-1
10XSTAT
AP-1
AP-1
F
DChepCA
18 h
Mmp1
AP-1
AP-1
Mmp1
G
Total AP-1
Total 10xSTAT
H
STAT in AP-1 domain
Fluorescence (A.U.)
Time AHS
0h
12h
24h
36h
I
DChepCA
24 h
DRWNT
AP-1
PH3
AP-1
PH3
DRWNT
PH3
J
DChepCA
36 h
DRWNT
AP-1
PH3
AP-1
PH3
DRWNT
PH3
K
***
ns
**
ns
ns
ns
PH3 positive cells
Wound center
Wound periphery
18 h
24 h
36 h
Time AHS
L
DCNA
DRWNT
10XSTAT
Mmp1
DRWNT
10XSTAT
Mmp1
M
DChepCA
18 h
DRWNT
10XSTAT
Mmp1
DRWNT
10XSTAT
Mmp1
N
DChepCA
24 h
DRWNT
10XSTAT
Mmp1
DRWNT
10XSTAT
Mmp1

Figure 3: DR^{WNT} overlaps with dynamic changes in JNK and JAK/STAT expression during regeneration.

(A-D) Regeneration time course of discs ablated by DC^{hepCA} and imaged at 0, 6, 12 and 18 h AHS. Discs bear the 10XSTAT reporter of JAK/STAT activity (*10XSTAT-dGFP*, green) and AP-1 reporter of JNK activity (*AP-1-RFP*, red). Cell death is labeled by Dcp-1 (white). (A) At 0 h AHS both reporters have only developmental expression, JAK/STAT in the hinge and JNK in the notum. (B) At 6 h AHS, JNK activity is observed alongside dying cells labelled by Dcp-1 in the distal pouch (yellow arrowhead). JAK/STAT is unchanged at this time point. (C) At 12 h AHS, JAK/STAT and JNK activity are both observed in the same cells of the distal pouch (yellow arrowhead). (D) At 18 h AHS, JAK/STAT is non-autonomously upregulated outside of the ablation domain (yellow arrowhead) where JNK activity does not occur (open arrowhead). **(E)** Magnified view of discs as in (D), showing JNK activity (AP-1 reporter, red) occurs in discrete high and low levels (yellow arrowheads, dotted outline) within the distal pouch, with non-autonomous JAK/STAT (10XSTAT reporter, green) occurring in the periphery. (**F**) Magnified view of discs as in (D), showing activity of the JNK target *Mmp1* (green) in relation to the high and low levels of JNK (dotted outline). **(G)** Quantification of JNK (AP-1 reporter) and JAK/STAT (10XSTAT reporter) activity based on fluorescent intensity in the pouch normalized to background following ablation at 6, 12, 18 ,24, 36 h AHS. n = 3-5 discs per time point, error bars are SD. **(H)** Quantification of JAK/STAT activity occurring within the JNK domain, measured as in (G), showing damage-induced JAK/STAT coincides with JNK initially before being downregulated within the JNK domain and upregulated outside of it. n = 3-5 discs per time point, error bars are SD. (**I-J)** Discs ablated by DC^{hepCA} bearing the JNK reporter (AP-1, red), the DR^{WNT} reporter (cyan) and stained for a marker of cell proliferation (PH3, white), imaged at 24 h AHS (I) and 36 h AHS (J). High levels of JNK (green dashed outline) lack proliferation at 24 h, which is restored by 36 h, while low JNK cells (yellow dashed outline) in the periphery of the wound have ongoing proliferation. **(K)** Quantification of proliferation within the high JNK and low JNK areas of the wound assayed by the number of PH3-positive cells. During early

regeneration (18 – 24 h) high JNK cells have significantly lower rates of proliferation, consistent with a proliferative pause, which recovers by 36 hours AHS. Proliferation of cells with lower JNK in the wound periphery increase over time, but changes are not statistically significant. Ordinary one-way ANOVA **p = 0.006, ***p = 0.0004, ns = not significant. n = 6-9 discs per timepoint, error bars are SD. **(L-N)** Discs bearing the DR^{WNT} reporter (cyan), JAK/STAT reporter (10XSTAT, green) and stained for the JNK target gene *Mmp1* (red), ablated by DC^{hepCA} (M and N) or unablated (DC^{NA}, L). Ablated discs imaged at 18 h AHS show that the DR^{WNT} reporter overlaps with JNK signaling, indicated by Mmp1 (red), which expands to also encompass the area of JAK/STAT signaling (green) at 24 h AHS (yellow dashes outline DR^{WNT} activity). Scale bars in all panels = 50 μm, except (E-F) = 14 μm, (L-N) = 18 μm.

Figure 4

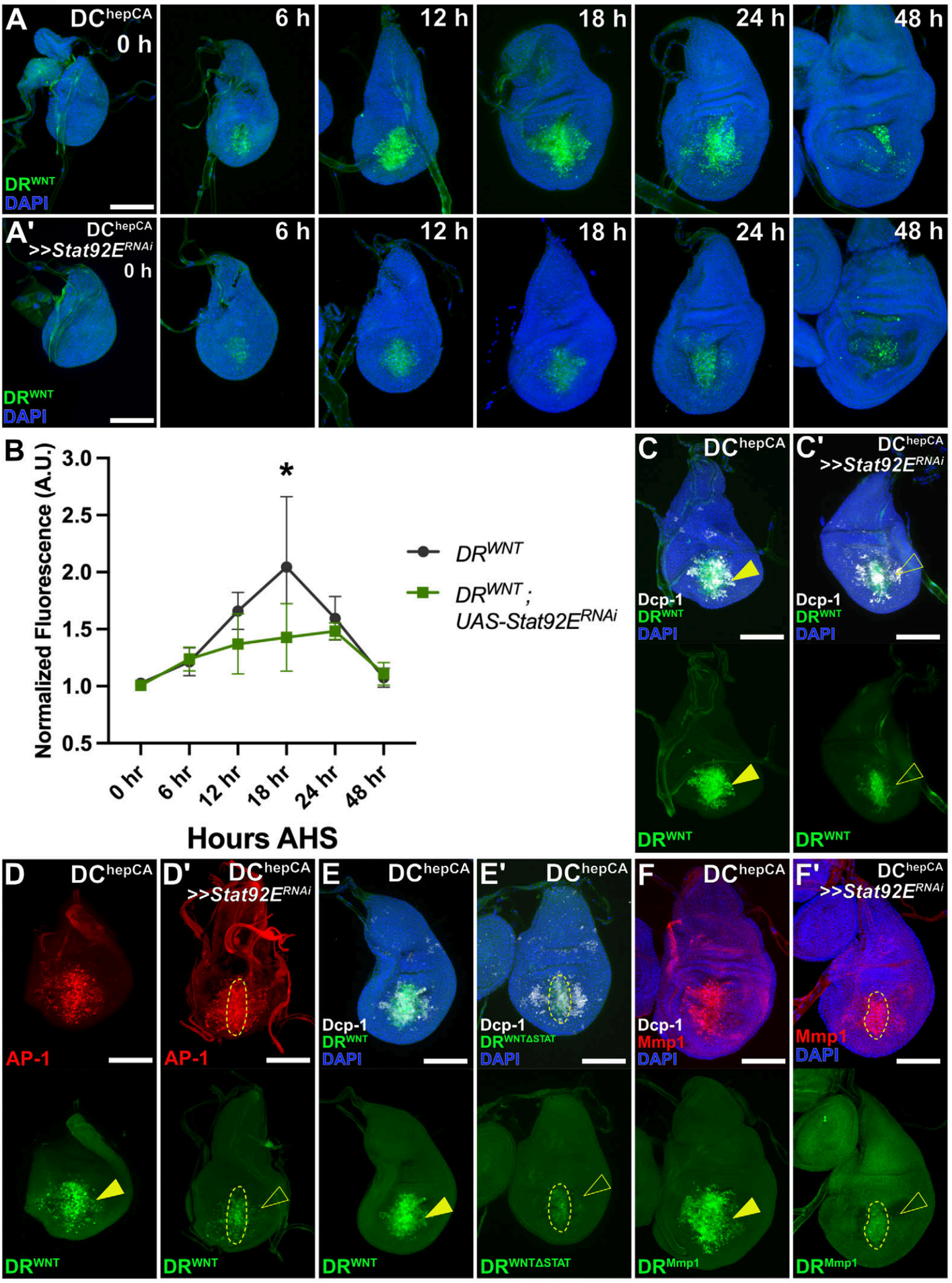
A
DC^hepCA
0 h
6 h
12 h
18 h
24 h
48 h
DR^WNT
DAPI
A'
DC^hepCA
>>Stat92E^RNAi
B
Normalized Fluorescence (A.U.)
3.0
2.5
2.0
1.5
1.0
0.5
*
0 hr
6 hr
12 hr
18 hr
24 hr
48 hr
Hours AHS
DR^WNT
DR^WNT ; UAS-Stat92E^RNAi
C
C'
Dcp-1
D
D'
E
E'
F
F'
AP-1
DR^WNTΔSTAT
Mmp1
DR^Mmp1

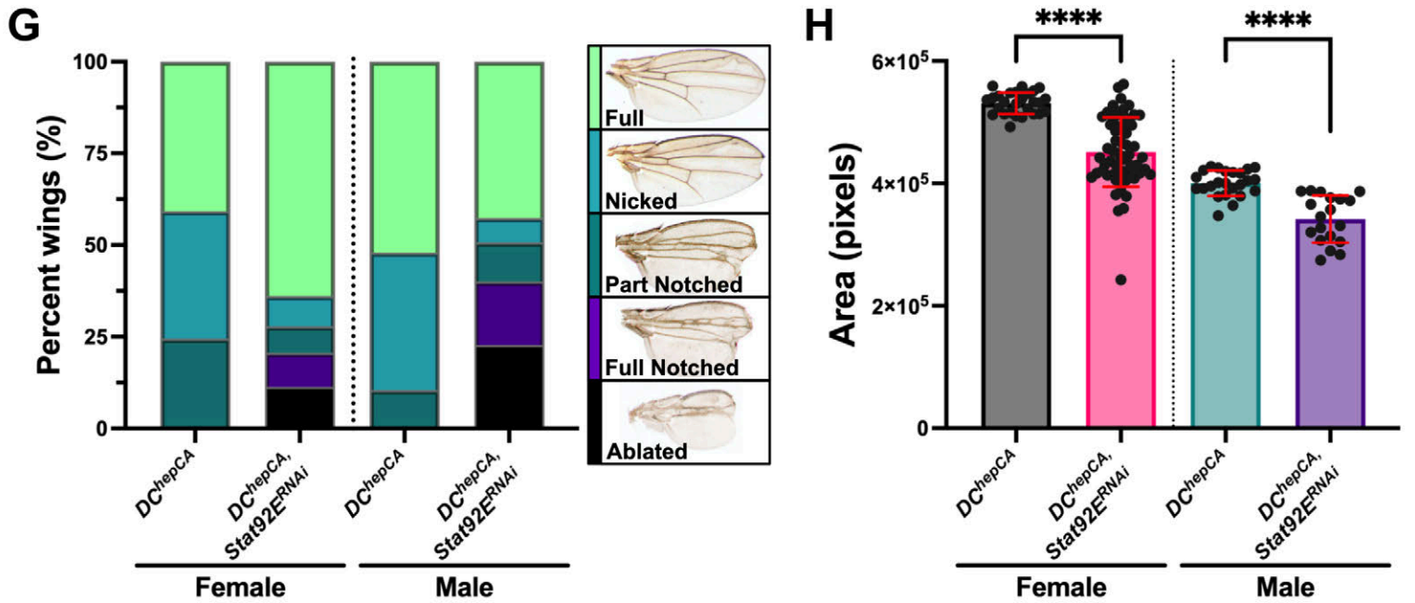
G
Percent wings (%)
100
75
50
25
0
DC^hepCA
DC^hepCA, Stat92E^RNAi
Female
Male
Full
Nicked
Part Notched
Full Notched
Ablated
H
Area (pixels)
6×10^5
4×10^5
2×10^5
0
****
****

Figure 4: Stat92E is necessary for full activation and lateral domain activity of DR^{WNT}.

(A-A') Time course of discs bearing the DR^{WNT} reporter ablated by DC^{HepCA} and imaged at 0, 6, 12, 18, 24, and 48 h AHS comparing wild type regeneration (A) to regeneration with knockdown of *Stat92E* (A'). **(B)** Quantification of DR^{WNT} reporter activity in (A) and (A') based on fluorescence intensity normalized to background, showing reduced activity upon *Stat92E* knockdown, with a statistically significant difference at 18 h AHS. Multiple t-test, *p = 0.0293 n = 3-9 discs per timepoint. **(C-C')** Discs bearing the DR^{WNT} reporter (green) ablated by DC^{HepCA}, stained for Dcp-1 (white) to show cell death, and imaged at 18 h AHS, comparing wild type regeneration (C) to regeneration with knockdown of *Stat92E* (C') highlighting the lack of lateral DR^{WNT} activity (yellow arrowhead in C, open arrowhead in C'). **(D-D')** Discs as in (C-C') with the JNK reporter (AP-1, red). The lateral DR^{WNT} activity (yellow arrowhead in D) that occurs outside of the region of high JNK (yellow dashed outline) is lost upon *Stat92E* knockdown (open arrowhead in D'). **(E-E)** Discs bearing the DR^{WNT} reporter (E) or the DR^{WNT} reporter with *Stat92E* binding sites deleted (*$DR^{WNT\Delta STAT}$-GFP*, E'), ablated by DC^{hepCA} and imaged at 18 h AHS. $DR^{WNT\Delta STAT}$ activity is absent from the lateral domain (open arrowhead in E') outside of high JNK cells (yellow dashed outline). (**F-F'**) Discs bearing the DR^{Mmp1} reporter (*DR^{MMP1}-GFP*, green) ablated by DC^{HepCA}, stained for Mmp1 (red) to show JNK activity, and imaged at 18 h AHS, comparing wild type regeneration (F) to regeneration with knockdown of *Stat92E* (F'). The lateral DR^{Mmp1} activity (yellow arrowhead in F) outside of the high JNK regions (yellow dashed outline) is absent from ablated discs with *Stat92E* knockdown (open arrowhead in F'). **(G)** Assay of adult wing phenotype scoring (categories shown right), following ablation by DC^{HepCA} in the presence of absence of *Stat92E* knockdown, showing a decreased regenerative capacity in the absence of JAK/STAT. Data separated by sex. n = 127 (*DC^{hepCA}*), n = 172 (*DC^{hepCA}*, *$Stat92E^{RNAi}$*). **(H)** Measurements of adult wing following ablation by DC^{HepCA} in the presence of absence of *Stat92E* knockdown, showing reduced wing size in the absence of

JAK/STAT. Data separated by sex. Unpaired two tailed t-tests, ****$p<0.0001$, n = 51 (*DC*^{hepCA}), n = 78 (*DC*^{hepCA}, *Stat92E*^{RNAi}). Scale bars in all panels = 50 μm.

Figure 5

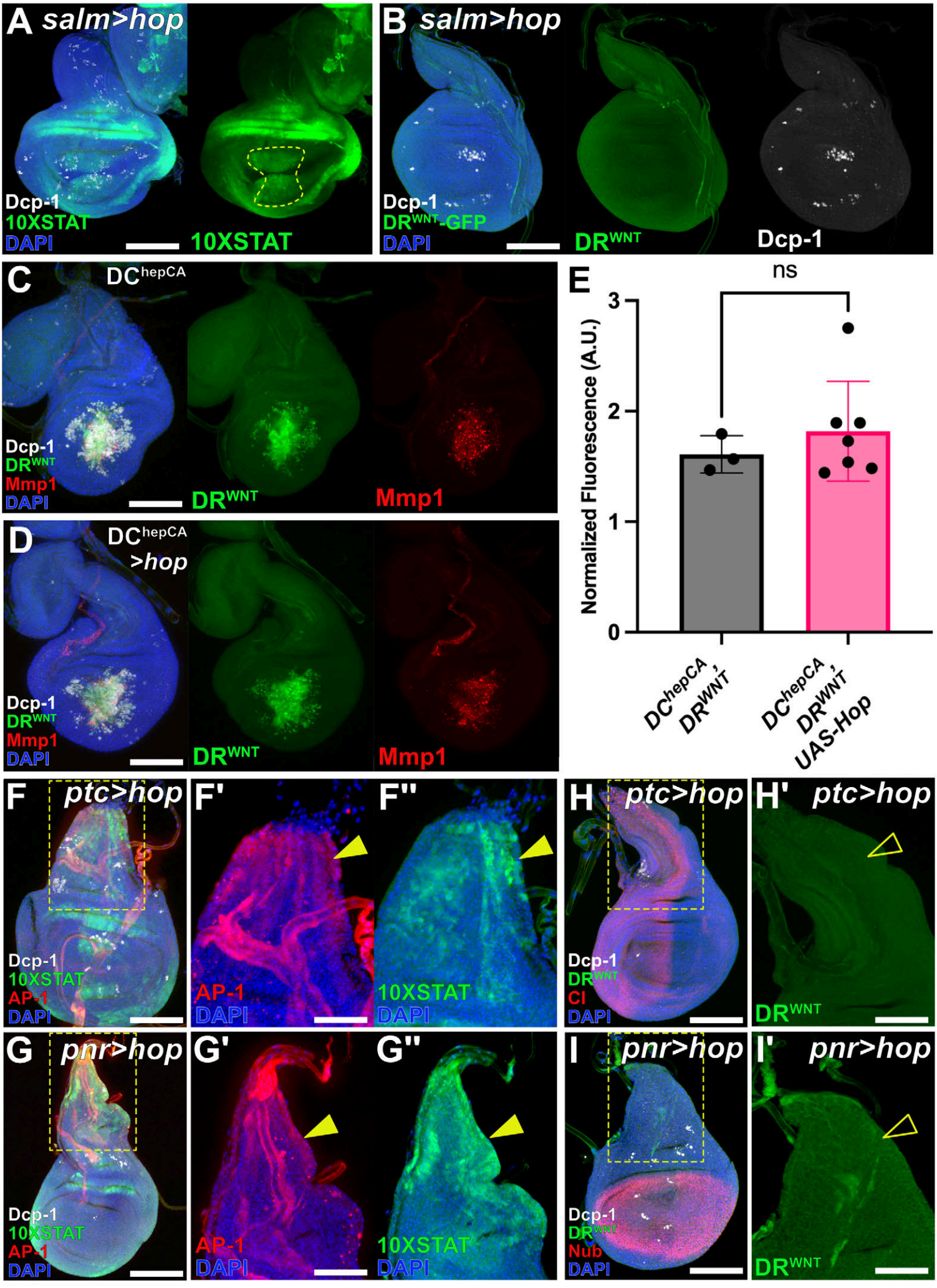
A salm>hop
Dcp-1
10XSTAT
DAPI
10XSTAT
B salm>hop
Dcp-1
DRWNT-GFP
DAPI
DRWNT
Dcp-1
C DChepCA
Dcp-1
DRWNT
Mmp1
DAPI
DRWNT
Mmp1
D DChepCA >hop
Dcp-1
DRWNT
Mmp1
DAPI
DRWNT
Mmp1
E
ns
Normalized Fluorescence (A.U.)
0
1
2
3
DChepCA, DRWNT
DChepCA, DRWNT, UAS-Hop
F ptc>hop
Dcp-1
10XSTAT
AP-1
DAPI
F'
AP-1
DAPI
F''
10XSTAT
DAPI
H ptc>hop
Dcp-1
DRWNT
CI
DAPI
H' ptc>hop
DRWNT
G pnr>hop
Dcp-1
10XSTAT
AP-1
DAPI
G'
AP-1
DAPI
G''
10XSTAT
DAPI
I pnr>hop
Dcp-1
DRWNT
Nub
DAPI
I' pnr>hop
DRWNT

Figure 5: JAK/STAT alone is insufficient to activate DR^{WNT}

(A) Disc with ectopic JAK/STAT signaling in the distal pouch (dashed yellow outline) by overexpression of *hop* (*salm-GAL4, UAS-hop*), confirmed by activation of the *10XSTAT-dGFP* reporter (green). Dcp-1 (white) shows lack of cell death. (**B**) Disc as in (A) showing the DRWNT enhancer reporter (green) is not activated by ectopic JAK/STAT. (**C**) Discs ablated by DC^{hepCA} have significant cell death (Dcp-1, white), DR^{WNT} reporter activation (green) and JNK signaling indicated by Mmp1 (red). (**D**) Disc as in (C) with ectopic JAK/STAT signaling via overexpression of *hop*. DR^{WNT} reporter (green) and JNK activity (Mmp1, red) are unaffected by ectopic JAK/STAT. (**E**) Quantification of DR^{WNT} reporter activity in ablated discs with and without ectopic JAK/STAT signaling, assayed by DR^{WNT} reporter fluorescent intensity normalized to background, showing no significant difference (n = 3, [DC^{hepCA}, DR^{WNT}], n = 7 [DC^{hepCA}, DR^{WNT}, *UAS-hop*], unpaired two-tailed t-test, ns = non-significant. (**F-F''**) Discs with ectopic JAK/STAT signaling in an A/P boundary stripe through overexpression of *hop* (*ptc-GAL4, UAS-hop*), confirmed by *10XSTAT-dGFP* expression (green, yellow arrowheads in F''). The AP-1 reporter (red) also indicates an increase in JNK signaling in the notum (yellow arrowhead in F'), alongside developmental JNK activity. Dcp-1 (white) shows lack of cell death. Yellow dashed box in F indicates magnified section in F' and F'', showing separate red and green channels. (**G-G''**) Discs as in F-F'' with ectopic JAK/STAT driven in the notum (*pnr-GAL4, UAS-hop*), confirmed by *10XSTAT-dGFP* activation (green) and showing increase in JNK (*AP-1-RFP*, red). (**H-H'**) Disc as in F, showing DR^{WNT} (green) is not activated by ectopic JAK/STAT (open arrowhead in H'). The A/P boundary is indicated by Ci (red) and cell death by Dcp-1 (white). Yellow dashed box in H indicates magnified section in H', showing green channel alone. (**I**) Disc as in G, showing DR^{WNT} (green) is not activated by ectopic JAK/STAT in the notum (open arrowhead in I'). The disc pouch is indicated by nub (red) and cell death by Dcp-1 (white). Yellow dashed box in I indicates magnified section in I', showing green channel alone. Scale bars in all panels = 50 μm, except (F'-F'',G'-G'',H',I') = 37.5 μm.

Figure 6

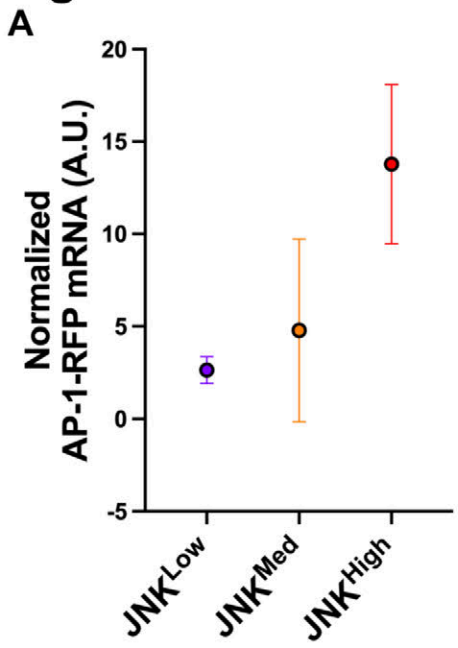
A
Normalized AP-1-RFP mRNA (A.U.)
20
15
10
5
0
-5
JNKLow
JNKMed
JNKHigh

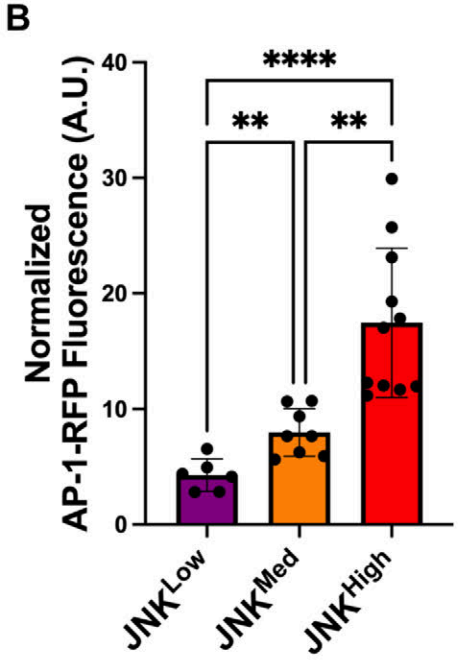
B
Normalized AP-1-RFP Fluorescence (A.U.)
40
30
20
10
0
****
**
**
JNKLow
JNKMed
JNKHigh

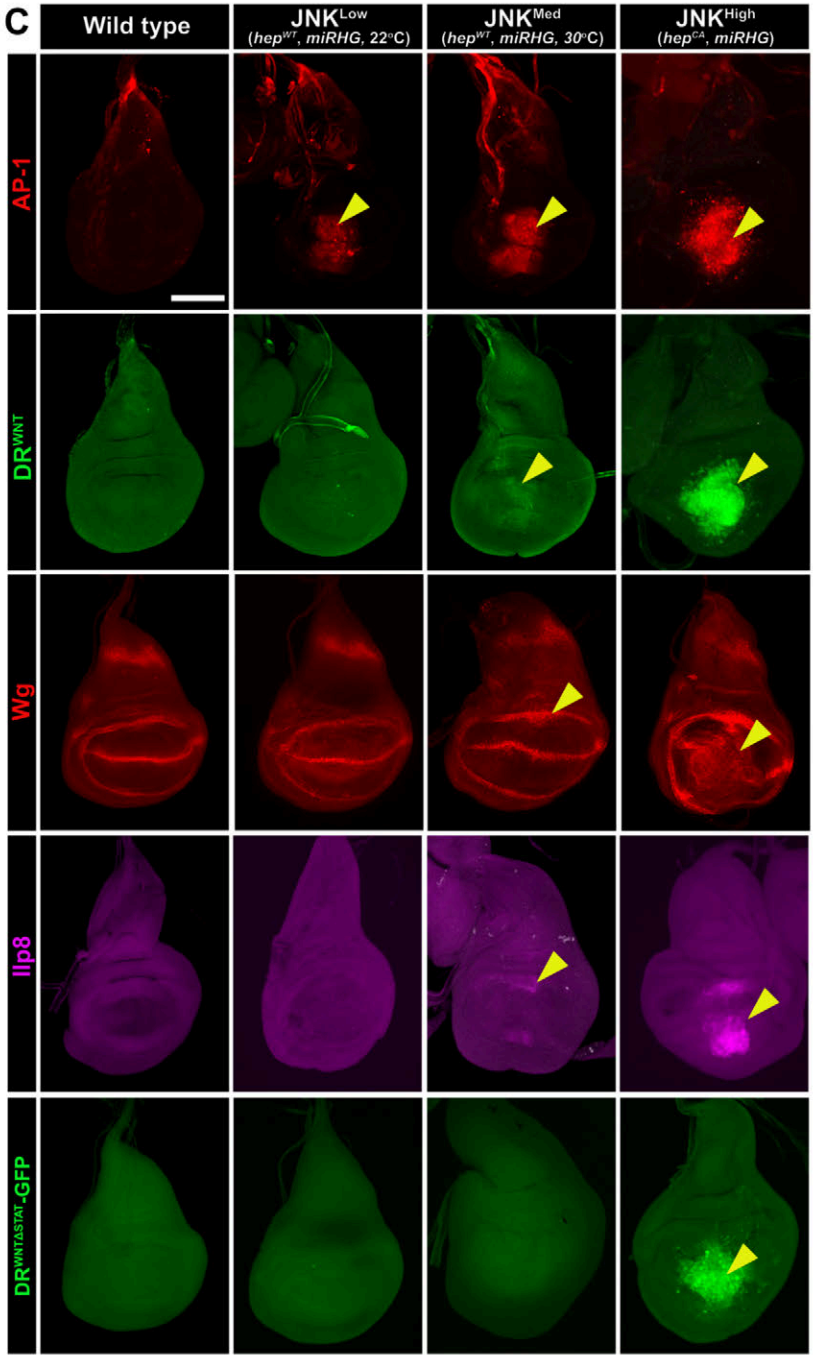
C
Wild type
JNKLow (hepWT, miRHG, 22°C)
JNKMed (hepWT, miRHG, 30°C)
JNKHigh (hepCA, miRHG)
AP-1
DRWNT
Wg
Ilp8
DRWNTASTAT-GFP

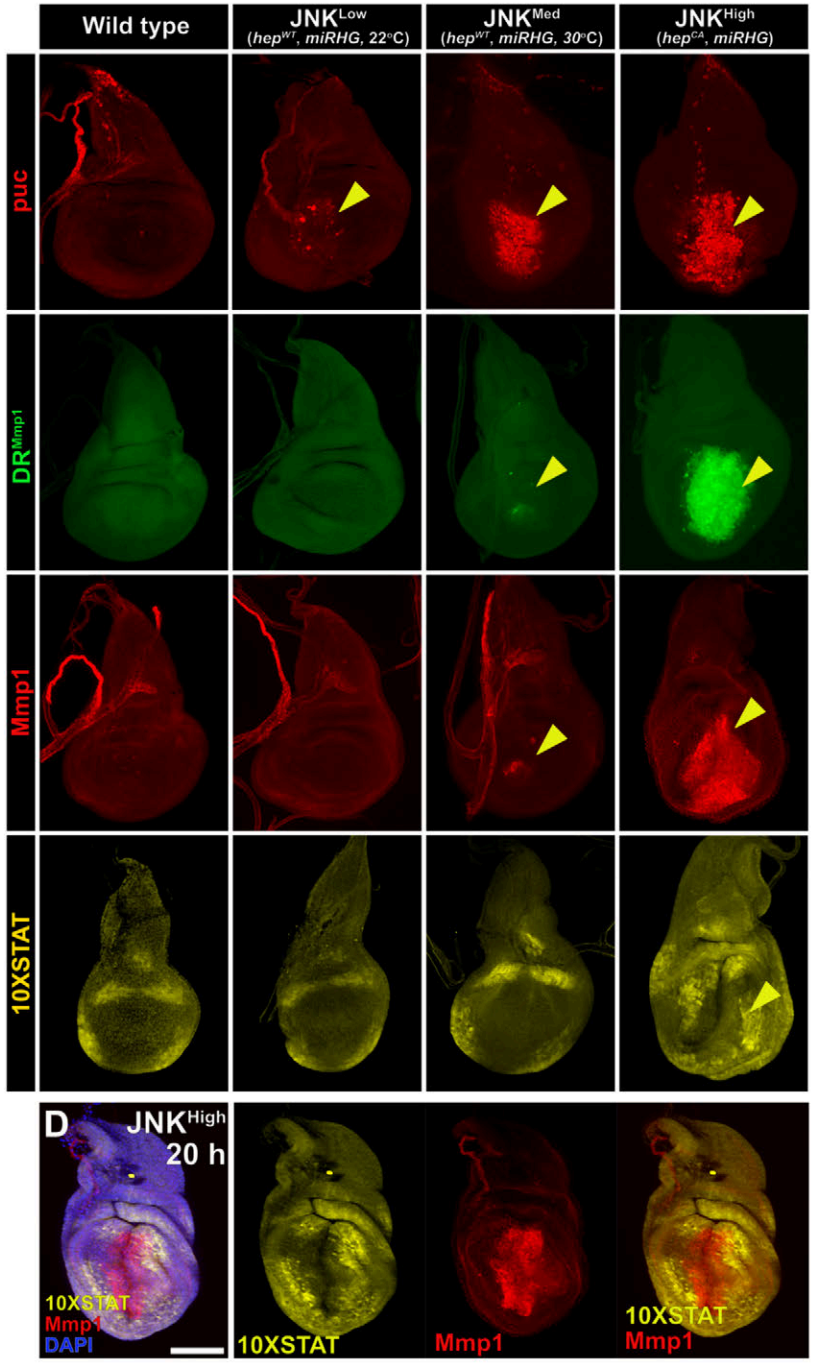
Wild type
JNKLow (hepWT, miRHG, 22°C)
JNKMed (hepWT, miRHG, 30°C)
JNKHigh (hepCA, miRHG)
puc
DRMmp1
Mmp1
10XSTAT
D
JNKHigh
20 h
10XSTAT
Mmp1
DAPI
10XSTAT
Mmp1
10XSTAT
Mmp1

Figure 6: A threshold level of JNK signaling is required for activation of the DR^{WNT} enhancer and downstream targets.

(A) Measurement of JNK levels in conditions of JNK^{Low} (*Salm-GAL4, UAS-hep^{WT}* at 22°C) JNK^{Med} (*Salm-GAL4, UAS-hep^{WT}* at 30°C) and JNK^{High} (*Salm-GAL4, UAS-hep^{CA}*) in the absence of cell death (*UAS-mir(RHG)*) by qRT-PCR of *AP-1-RFP* transcript levels. Graphs show the mean fold change of *AP-1 RFP* in each JNK condition relative to wild-type. n = 3 measurements per condition. **(B)** Measurement of JNK levels in conditions of JNK^{Low}, JNK^{Med} and JNK^{High} by fluorescent intensity of *AP-1-RFP* in the pouch normalized to background. Ordinary one-way ANOVA, **p=0.005 (JNK^{Low}-JNK^{Med}), **p=0.0016 (JNK^{Med}-JNK^{High}), ****p<0.0001. Error bars are SD, n = 6 discs (JNK^{Low}), 8 discs (JNK^{Med}) and 11 discs (JNK^{High}), **(C)** Reporters of gene and reporter expression related to regeneration in wildtype, JNK^{Low}, JNK^{Med}, and JNK^{High} conditions. Reporters of JNK signaling, (*AP-1-RFP* and *puc-LacZ*) are activated at all JNK levels (yellow arrowheads). The DR^{WNT} reporter, DR^{Mmp1} reporter, Mmp1 and Ilp8 are are weakly activated at JNK^{Med} and strongly at JNK^{High} (yellow arrowheads). The 10XSTAT reporter is only activated at JNK^{High}. **(D)** Discs under JNK^{High} conditions bearing 10XSTAT reporter (yellow) and the JNK target Mmp1 (red). The expression of each becomes mutually exclusive, emulating a late-stage wound. Scale bar in all panels = 50 μm.

Figure 7

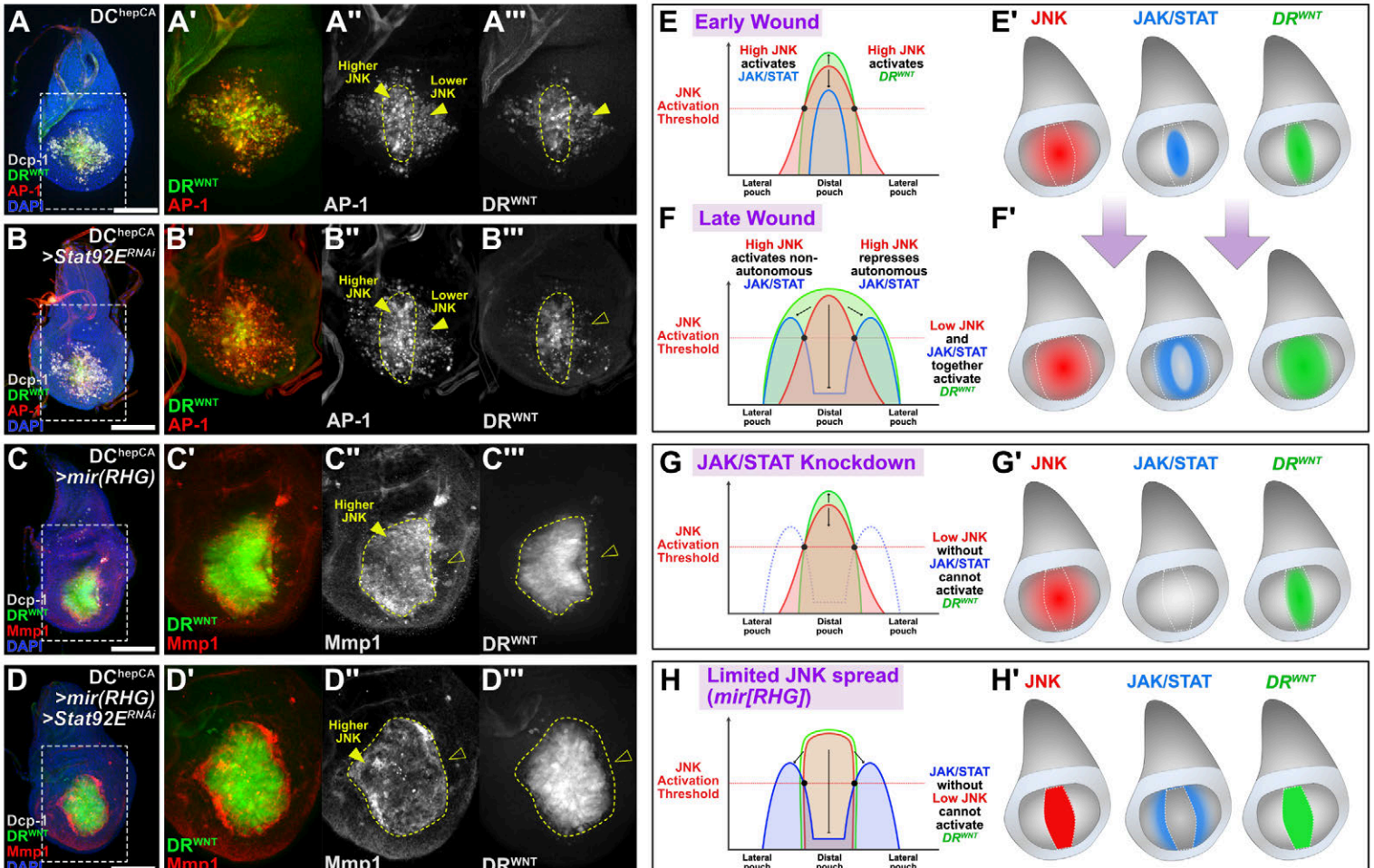
A
DC^hepCA
Dcp-1
DR^WNT
AP-1
DAPI
A'
DR^WNT
AP-1
A''
Higher JNK
Lower JNK
AP-1
A'''
DR^WNT
B
DC^hepCA >Stat92E^RNAi
Dcp-1
DR^WNT
AP-1
DAPI
B'
DR^WNT
AP-1
B''
Higher JNK
Lower JNK
AP-1
B'''
DR^WNT
C
DC^hepCA >mir(RHG)
Dcp-1
DR^WNT
Mmp1
DAPI
C'
DR^WNT
Mmp1
C''
Higher JNK
Mmp1
C'''
DR^WNT
D
DC^hepCA >mir(RHG) >Stat92E^RNAi
Dcp-1
DR^WNT
Mmp1
DAPI
D'
DR^WNT
Mmp1
D''
Higher JNK
Mmp1
D'''
DR^WNT
E
Early Wound
High JNK activates JAK/STAT
High JNK activates DR^WNT
JNK Activation Threshold
Lateral pouch
Distal pouch
Lateral pouch
E'
JNK
JAK/STAT
DR^WNT
F
Late Wound
High JNK activates non-autonomous JAK/STAT
High JNK represses autonomous JAK/STAT
JNK Activation Threshold
Low JNK and JAK/STAT together activate DR^WNT
Lateral pouch
Distal pouch
Lateral pouch
F'
G
JAK/STAT Knockdown
JNK Activation Threshold
Low JNK without JAK/STAT cannot activate DR^WNT
Lateral pouch
Distal pouch
Lateral pouch
G'
JNK
JAK/STAT
DR^WNT
H
Limited JNK spread (mir[RHG])
JNK Activation Threshold
JAK/STAT without Low JNK cannot activate DR^WNT
Lateral pouch
Distal pouch
Lateral pouch
H'
JNK
JAK/STAT
DR^WNT

Figure 7: JNK and JAK/STAT expression dynamically activates DR^{WNT} during early and late wound formation.

(A-D''')) Discs bearing the DR^{WNT} reporter (green) and the AP-1 reporter (red in A and B) or stained for JNK target Mmp1 (red in C and D), ablated by DC^{HepCA}. Discs are wild type (A), with *Stat92E* knockdown (B), with cell death blocked by *mir(RHG)* (C) or with *Stat92E* and cell death block by *mir(RHG)* together (D). DR^{WNT} activity occurs in cells of both high and low JNK of a wound (A-A'), while lack of JAK/STAT limits DR^{WNT} activity to cells with high JNK (B-B'''). Blocking cell death via mir(RHG) to inhibit ROS-mediated spread of JNK prevents the formation of a low JNK area where JAK/STAT can be activated, and therefore DR^{WNT} is limited to the high JNK cells in the center of the distal pouch (C-C'''). Preventing the spread of JNK via blocking cell death with *mir(RHG)* and blocking JAK/STAT shows the same lack of DR^{WNT} activity outside of the distal pouch (D-D'''). Limited JNK spread is shown by Mmp1 staining in C and D. Yellow dashed outlines indicate area of high JNK. Yellow arrowheads indicate high JNK cells in the center of the wound and lower JNK cells in the wound periphery. Open arrowheads indicate lack of DR^{WNT} activity in B''', C''' and D'''', and lack of JNK activity shown by Mmp1 in C'' and D''. (**E-H'**) Graphical representation of how JNK and JAK/STAT expression leads to DR^{WNT} activity across a developing wound (E-F'), and in conditions of JAK/STAT knockdown (G-G') or when JNK signaling spread is prevented (H-H'). See main text for details. Scale bars in (A-D) = 50 μm, (A'-D''') = 37.5 μm.

Supporting Information Captions

S1 Fig: Ablation activates DR^{WNT} and causes overgrowth in the absence of cell death.

(**A**) Wing imaginal disc bearing the DR^{WNT} reporter (green), ablated by DC^{HepCA} and expressing *lexAop-RFP* (red) to label the ablation domain, stained with Dcp-1 (white) to show cell death. DR^{WNT} overlaps RFP, and ablation is consistent across the pouch. Yellow arrowheads point to regenerating cells with DR^{WNT} activity and no Dcp-1. **(B)** Wing imaginal disc bearing the DR^{WNT} reporter (green), ablated by DC^{HepCA} and stained for Mmp1 (red). Yellow arrowheads and open arrowheads indicate cells with DR^{WNT} reporter activity that do not have Mmp1. **(C)** The notum of the wing discs showing the developmental expression of the AP-1 reporter, the 10XSTAT reporter, Mmp1, Ilp8, Wg, Mol reporter. Yellow arrowheads indicate expression, and an open arrowhead points to the lack of expression. (**E**) Quantification of pouch size using the tissue folds in the hinge as a marker for the pouch in non-ablated (DC^{A}) and ablated discs in which cell death is blocked by *mir(RHG)* (DC^{hepCA}, mir(RHG)), showing mild but significant overgrowth. Error bars are SD. n = 11, (DC^{NA}), n = 10 (DC^{hepCA}, *mir(RHG)*), unpaired two-tailed t-test, **p = 0.004. Scale bars = 50 μm.

S2 Fig: Whole genome analysis of early and late L3 discs identifies changes in factors associated with JNK signaling.

(**A**) Analysis of motif enrichment (AME) performed on DR regions identified in early L3 discs and late L3 discs by ATAC-seq. 243 DR regions were analyzed with 12,779 static peaks as control sequences. Enrichment is shown as -LOG10 adj p value. (**B-C**) Volcano plots of differentially expressed genes induced by damage identified by RNA-seq. LOG_2 fold change (LOG_2FC) vs. significance ($-LOG_{10}$ adjusted p-value) of genes expressed in (C) early and (D) late L3 stages between damaged vs. undamaged conditions. JNK related genes are labelled. (**D**) Heatmap of the expression levels of JNK

pathway genes across each stage (early vs late), damage condition (undamaged versus damaged) and replicate (first or second biological repeat), with red representing higher expression and blue representing lower expression. (**E**) Heatmap comparing damage-induced fold change (LOG_2FC) of genes related to JNK signaling, including the ligands, pathway transducers, target genes and known negative regulators in early L3 versus late L3 discs. Gray cells indicate p-value is not significant ($p>0.05$).

S3 Fig: JNK and JAK/STAT signaling occur dynamically during regeneration.

(**A**) Full time course of discs ablated by DC^{hepCA} and imaged at 0, 6, 12, 18, 24, 36 h AHS during regeneration. Discs bear the 10XSTAT reporter of JAK/STAT activity (*10XSTAT-dGFP*, green) and AP-1 reporter of JNK activity (AP-1-RFP, red). Cell death is labeled by Dcp-1 (white). **(B)** Disc bearing the 10XSTAT reporter (green) and DR^{WNT} reporter (cyan) ablated with DC^{hepCA}, stained for Mmp1 and imaged at 36 AHS, showing the diminished expression of these factors in late regeneration. Scale bars in all panels = 50 μm, except (B) = 45 μm.

S4 Fig: Other DR/DRMS reporters are activated by damage, but not altered by JAK/STAT signaling.

(**A**) Schematic of the $DRMS^{Mmp1}$ regulatory element (top), showing the separable damage-responsive (DR) region that activates *Mmp1* expression upon damage, and the maturity-silencing (MS) region that limits DR activity with developmental maturity. The DR^{Mmp1} reporter (bottom), comprising the DR^{Mmp1} enhancer DNA, *hsp70* promoter and GFP coding sequence. Schematic shows AP-1 and Stat92E transcription factor binding sites in the DR^{Mmp1} region, with details shown in table (right). (**B**) Quantification of DR^{Mmp1} reporter activity assayed by fluorescence intensity normalized to background in DC^{hepCA} ablated discs and DC^{hepCA} ablated discs with JAK/STAT blocked via *Stat92E* knockdown.

Error bars are SD. n = 6 (DC^{hepCA}), n = 11 (DC^{hepCA}, *Stat92E*^{RNAi}), unpaired two-tailed t-test, **p = 0.0011. (**C**) Schematic of $DRMS^{TDC1/2}$ labelled as in (A). This reporter has no sites matching the Stat92E consensus (**D**) Discs bearing the $DRMS^{TDC1/2}$ reporter (*DRMS*$^{TDC1/2}$*-GFP*, green) ablated by DC^{hepCA} with and without *Stat92E* knockdown, showing no difference in damage-induced activity. (**E**) Quantification of $DRMS^{TDC1/2}$ reporter activity assayed by fluorescence intensity normalized to background in DC^{hepCA} ablated discs and DC^{hepCA} ablated discs with JAK/STAT blocked via *Stat92E* knockdown. Error bars are SD. n = 4 (DC^{hepCA}), n = 4 (DC^{hepCA}, *Stat92E*^{RNAi}), unpaired two-tailed t-test, ns = not significant. (**F**) Schematic showing the deletions of three potential Stat92E consensus binding sites to generate the $DR^{WNT\Delta STAT}$ reporter. (**G**) Quantification of $DR^{WNT\Delta STAT}$ reporter activity compared to DR^{WNT} assayed by fluorescence intensity normalized to background in DC^{hepCA} ablated discs. Error bars are SD. n = 3 (DC^{hepCA}, DR^{WNT}), n = 5 (DC^{hepCA}, $DR^{WNT\Delta STAT}$), unpaired two-tailed t-test, **p = 0.0014. Scale bars = 50 μm.

S5 Fig: JAK/STAT manipulation through *hop* expression.

A) Disc with ectopic JAK/STAT signaling in the distal pouch (dashed yellow outline) through overexpression of *hop* (*rn-GAL4*, *UAS-hop*), confirmed by activation of the 10XSTAT reporter (green). Dcp-1 (white) shows lack of cell death, Mmp1 (red) shows JNK activity **B**) Disc as in (A) showing the DR^{WNT} enhancer reporter (green) is not activated by ectopic JAK/STAT, **C**) Disc with ectopic JAK/STAT signaling in the posterior compartment (dashed yellow line shows A/P boundary) through overexpression of *hop* (*hh-GAL4*, *UAS-hop*), confirmed by activation of the 10XSTAT reporter (green). Asterisk highlights development of an ectopic pouch generated by JAK/STAT in the notum. (**D**) Disc with ectopic JAK/STAT signaling in the A/P boundary (dashed through overexpression of *hop* (*ptc-GAL4*, *UAS-hop*). Asterisk highlights development of an ectopic pouch generated by JAK/STAT in the notum, shown by nub staining (red). (**E**) Disc bearing the DR^{WNT} reporter (green) with high levels of JAK/STAT in the distal pouch through overexpression of the *hop*^{ORF} transgene (*salm-GAL4, UAS-hop*^{ORF}), which causes significant cell death, shown by Dcp-1 staining (white), and JNK activity shown

by Mmp1 (red). (**F**) Disc as in (E) bearing the 10XSTAT reporter (green), showing *hop*^{ORF} activates JAK/STAT signaling. (**G-H**) Discs with pannier-GAL4 (G) or patched-GAL4 (H) driving GFP (green) to demonstrate their expression domains (*pnr-GAL4, UAS-GFP*, or *ptc-GAL4, UAS-GFP*). Scale bar in all panels = 50 μm, except (H) = 45 μm.

S6 Fig: Production of ROS and expression of the ROS agonist *mol* following ablation and at different JNK levels.

(**A-D''**) Visualization of reactive oxygen species (ROS) shown by DHE in discs of the indicated genotype/condition. Yellow arrowheads indicate higher levels of ROS. Non-ablated discs (DC^{NA}) have no detectable ROS (A), while ablation with DC^{HepCA} leads to ROS production (B). ROS is not detected at any level of JNK activity when cell death is blocked by mir(RHG), which prevents JNK spreading (C-C''). Discs ablated as in (B) but with cell death blocked by mir(RHG) limits ROS production (D). Blocking JAK/STAT signaling by *Stat92E* knockdown does not change ROS production (D'), while additionally blocking cell death by mir(RHG) does prevent ROS (D''). (**E-F**) Discs bearing the mol reporter (*mol-lacZ*) in wild type conditions (DC^{NA}, E) or in different levels of JNK activity (F-F''), showing no change in reporter activity. Scale bars = 50 μm.

S1 Table: List of differentially expressed genes in damaged versus undamaged discs from early and late L3 larvae.

Genes that are differentially expressed upon damage in early and late L3 discs identified by RNA-seq. Data include unique Flybase gene ID, gene names and expression attributes.

S2 Table: Intersections of genes in damaged versus undamaged discs from early and late L3 larvae.

Grouping of genes showing their intersection across injury condition (damaged or undamaged) and developmental stage (early or late L3). Data include unique Flybase gene ID, gene names and expression attributes.

S1 Figure

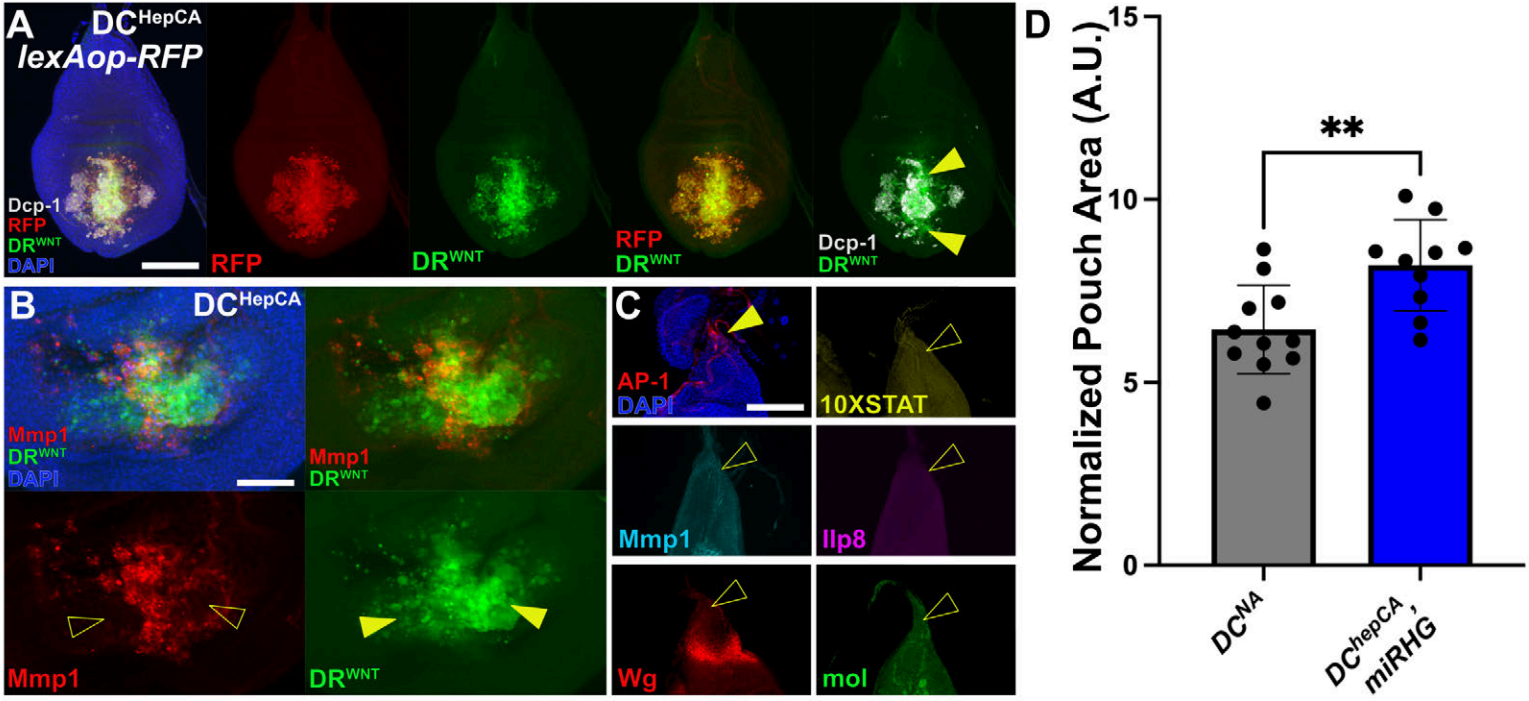
A
DC^HepCA
lexAop-RFP
Dcp-1
RFP
DR^WNT
DAPI
RFP
DR^WNT
RFP
DR^WNT
Dcp-1
DR^WNT
B
DC^HepCA
Mmp1
DR^WNT
DAPI
Mmp1
DR^WNT
Mmp1
DR^WNT
C
AP-1
DAPI
10XSTAT
Mmp1
Ilp8
Wg
mol
D
Normalized Pouch Area (A.U.)
15
10
5
0
**
DC^NA
DC^hepCA, miRHG

S2 Figure

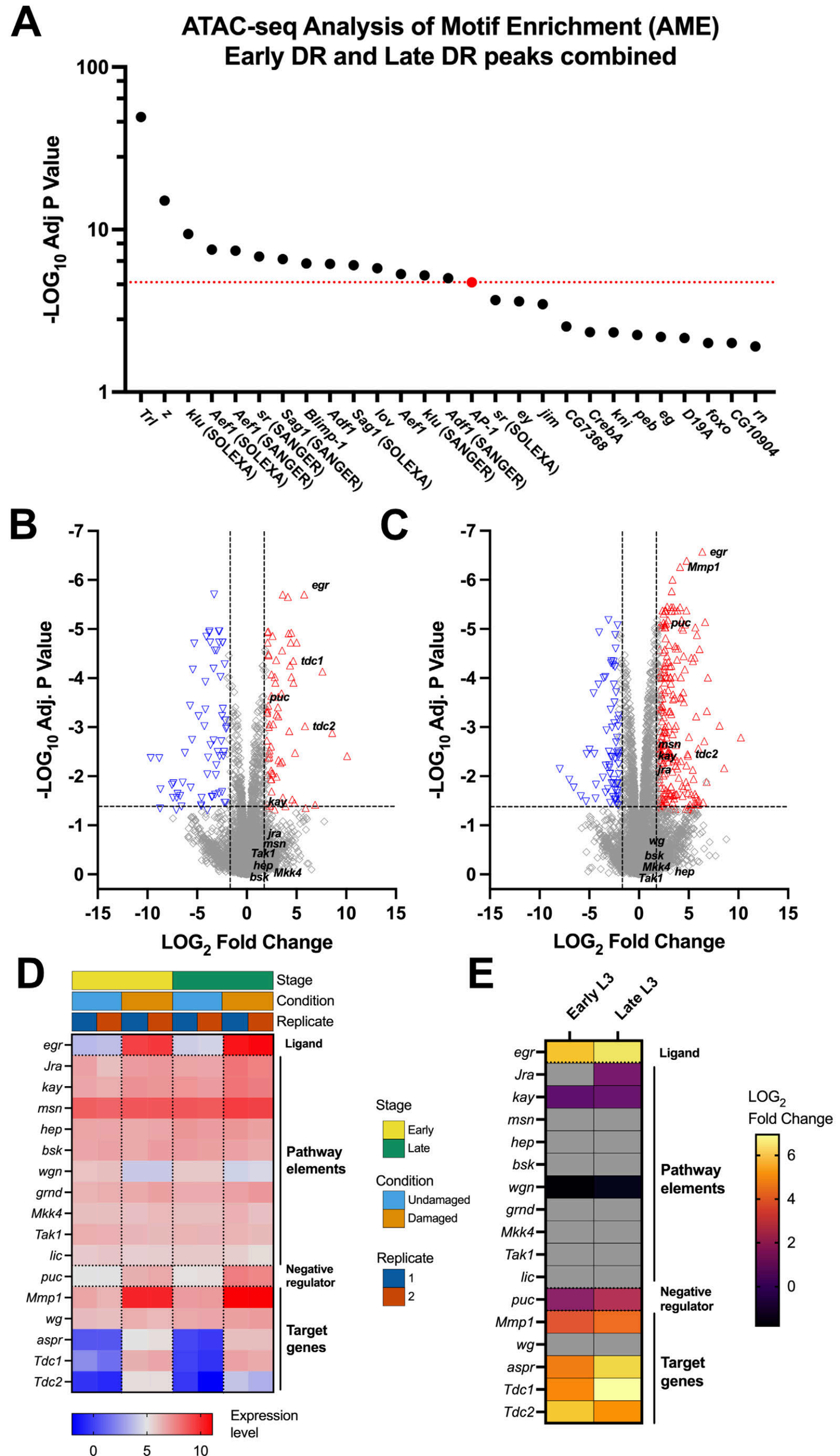
A
ATAC-seq Analysis of Motif Enrichment (AME)
Early DR and Late DR peaks combined
-LOG10 Adj P Value
100
10
1
Trl
z
klu (SOLEXA)
Aef1 (SOLEXA)
Aef1 (SANGER)
sr (SANGER)
Sag1 (SANGER)
Blimp-1
Adf1
Sag1 (SOLEXA)
lov
Aef1
klu (SANGER)
Adf1 (SANGER)
AP-1
sr (SOLEXA)
ey
jim
CG7368
CrebA
kni
peb
eg
D19A
foxo
CG10904
rn
B
-LOG10 Adj. P Value
LOG2 Fold Change
egr
tdc1
puc
tdc2
kay
jra
msn
Tak1
hep
bsk
Mkk4
C
-LOG10 Adj. P Value
LOG2 Fold Change
egr
Mmp1
puc
msn
kay
tdc2
jra
wg
bsk
Mkk4
Tak1
hep
D
Stage
Condition
Replicate
Ligand
Pathway elements
Negative regulator
Target genes
egr
Jra
kay
msn
hep
bsk
wgn
grnd
Mkk4
Tak1
lic
puc
Mmp1
wg
aspr
Tdc1
Tdc2
Stage
Early
Late
Condition
Undamaged
Damaged
Replicate
1
2
Expression level
0
5
10
E
Early L3
Late L3
Ligand
Pathway elements
Negative regulator
Target genes
egr
Jra
kay
msn
hep
bsk
wgn
grnd
Mkk4
Tak1
lic
puc
Mmp1
wg
aspr
Tdc1
Tdc2
LOG2 Fold Change
6
4
2
0

S3 Figure

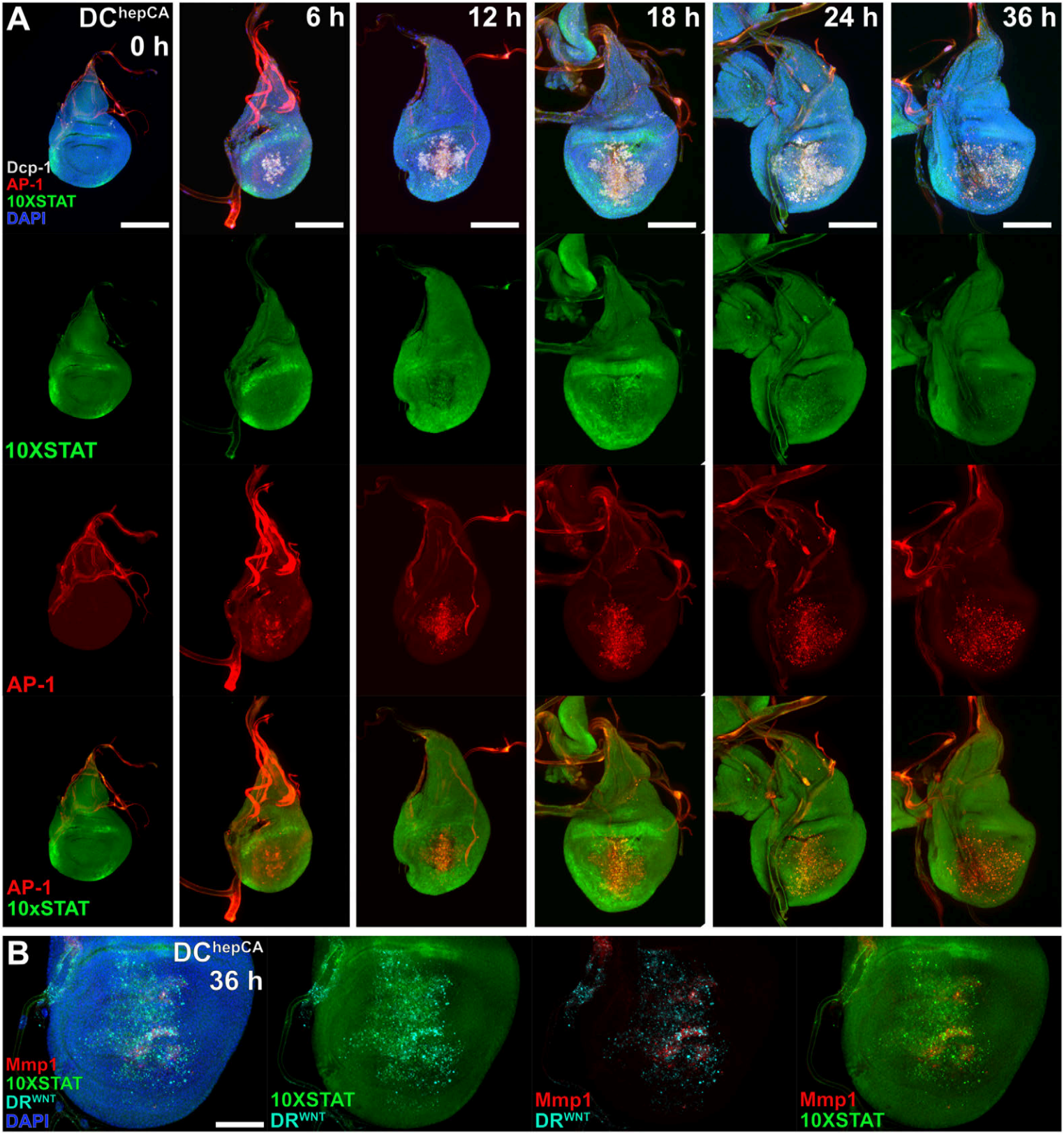
A
DC^hepCA
0 h
6 h
12 h
18 h
24 h
36 h
Dcp-1
AP-1
10XSTAT
DAPI
10XSTAT
AP-1
AP-1
10xSTAT
B
DC^hepCA
36 h
Mmp1
10XSTAT
DR^WNT
DAPI
10XSTAT
DR^WNT
Mmp1
DR^WNT
Mmp1
10XSTAT

S4 Figure

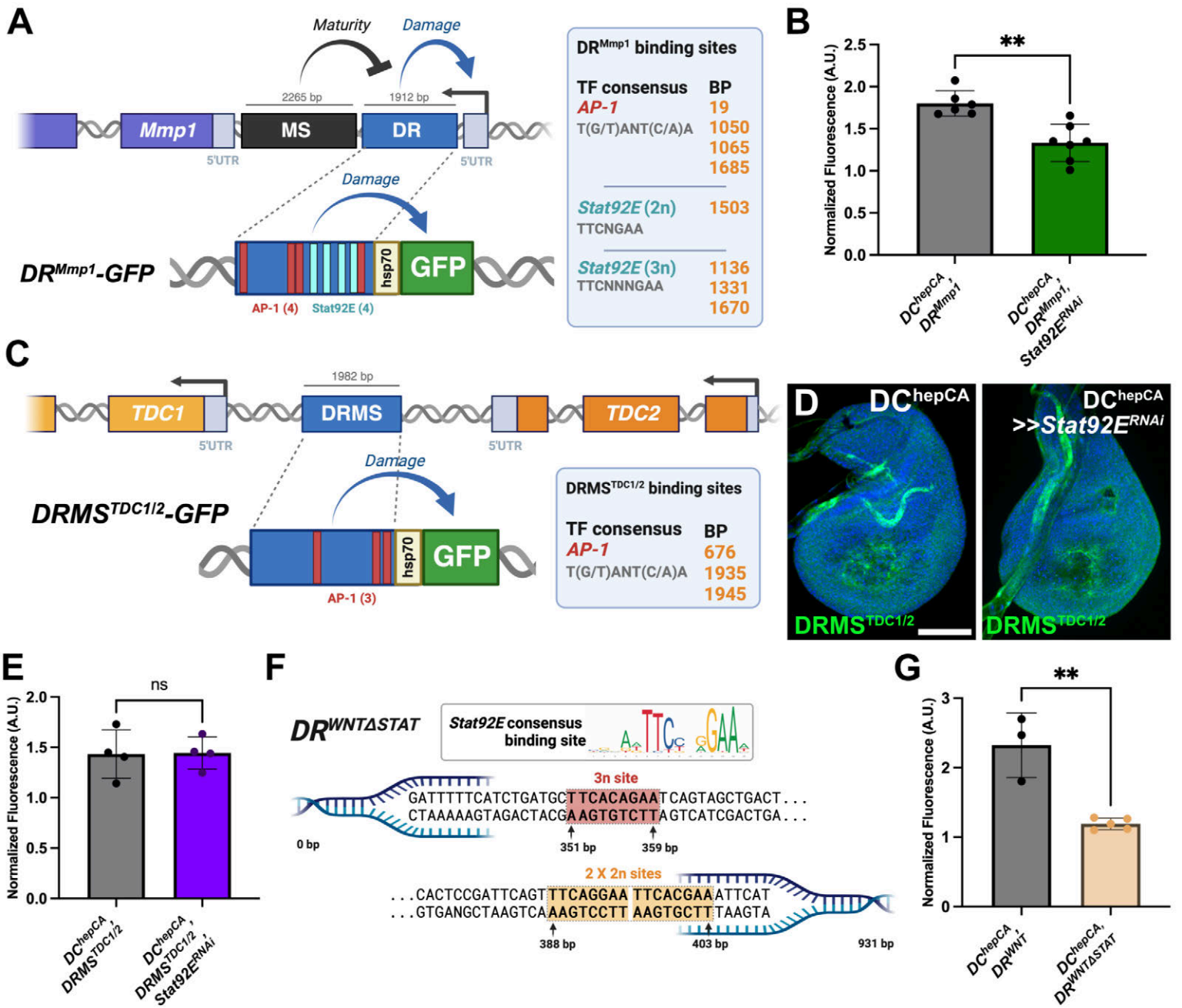
A
Maturity
Damage
2265 bp
1912 bp
Mmp1
MS
DR
5'UTR
5'UTR
Damage
DRMmp1-GFP
hsp70
GFP
AP-1 (4)
Stat92E (4)
DRMmp1 binding sites
TF consensus
BP
AP-1
T(G/T)ANT(C/A)A
19
1050
1065
1685
Stat92E (2n)
TTCNGAA
1503
Stat92E (3n)
TTCNNNGAA
1136
1331
1670
B
Normalized Fluorescence (A.U.)
2.5
2.0
1.5
1.0
0.5
0.0
**
DChepCA, DRMmp1
DChepCA, DRMmp1, Stat92ERNAi
C
1982 bp
TDC1
DRMS
TDC2
5'UTR
5'UTR
Damage
DRMSTDC1/2-GFP
hsp70
GFP
AP-1 (3)
DRMSTDC1/2 binding sites
TF consensus
BP
AP-1
T(G/T)ANT(C/A)A
676
1935
1945
D
DChepCA
DChepCA >>Stat92ERNAi
DRMSTDC1/2
DRMSTDC1/2
E
Normalized Fluorescence (A.U.)
2.0
1.5
1.0
0.5
0.0
ns
DChepCA, DRMSTDC1/2
DChepCA, DRMSTDC1/2, Stat92ERNAi
F
DRWNTΔSTAT
Stat92E consensus binding site
3n site
GATTTTTCATCTGATGCTTCACAGAATCAGTAGCTGACT...
CTAAAAAGTAGACTACGAAGTGTCTTAGTCATCGACTGA...
0 bp
351 bp
359 bp
2 X 2n sites
...CACTCCGATTCAGTTTCAGGAA TTCACGAAATTCAT
...GTGANGCTAAGTCAAAGTCCTT AAGTGCTTTAAGTA
388 bp
403 bp
931 bp
G
Normalized Fluorescence (A.U.)
3
2
1
0
**
DChepCA, DRWNT
DChepCA, DRWNTΔSTAT

S5 Figure

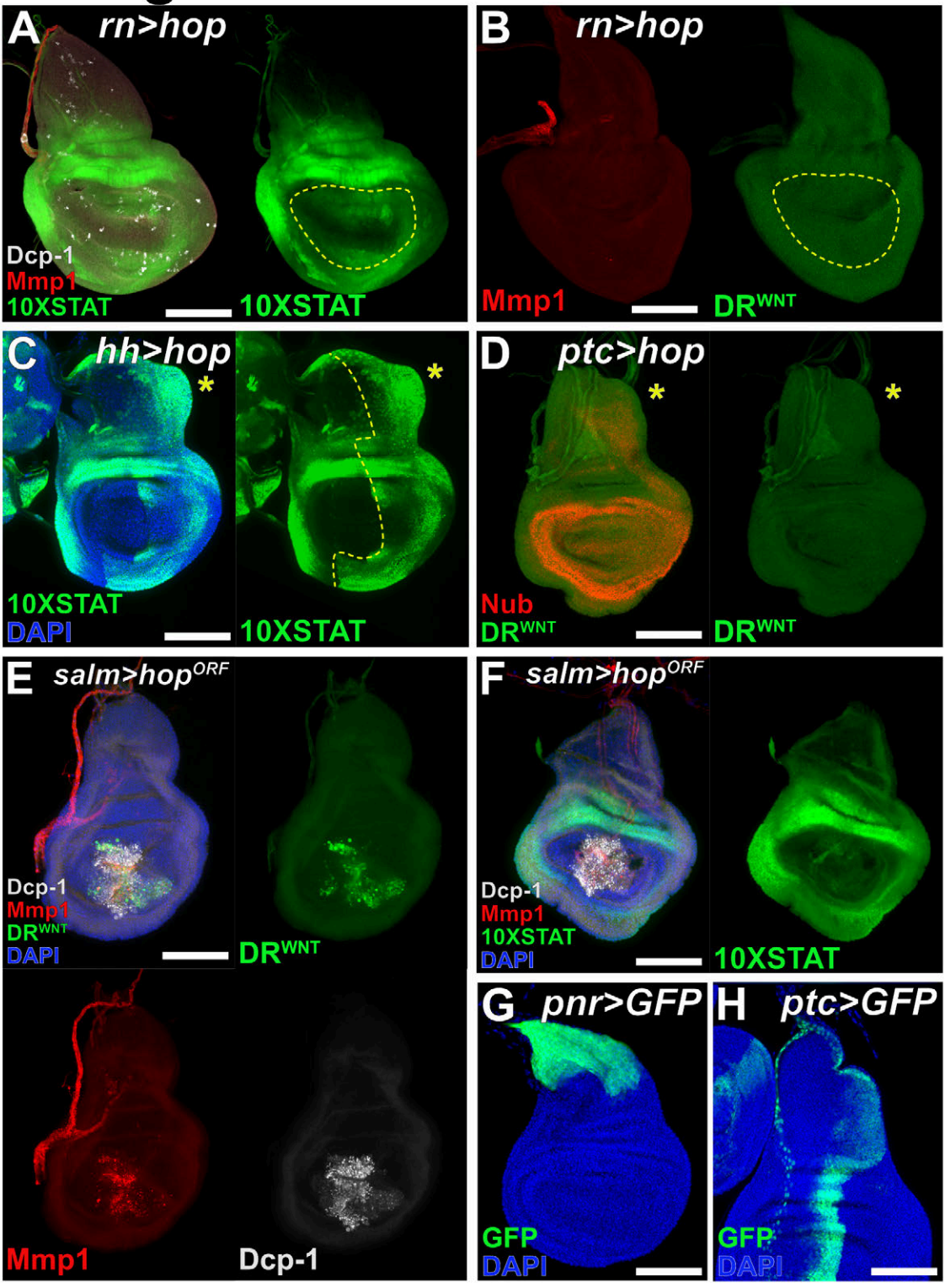
A
rn>hop
Dcp-1
Mmp1
10XSTAT
10XSTAT
B
rn>hop
Mmp1
DR^WNT
C
hh>hop
*
*
10XSTAT
DAPI
10XSTAT
D
ptc>hop
*
*
Nub
DR^WNT
DR^WNT
E
salm>hop^ORF
Dcp-1
Mmp1
DR^WNT
DAPI
DR^WNT
Mmp1
Dcp-1
F
salm>hop^ORF
Dcp-1
Mmp1
10XSTAT
DAPI
10XSTAT
G
pnr>GFP
GFP
DAPI
H
ptc>GFP
GFP
DAPI

S6 Figure

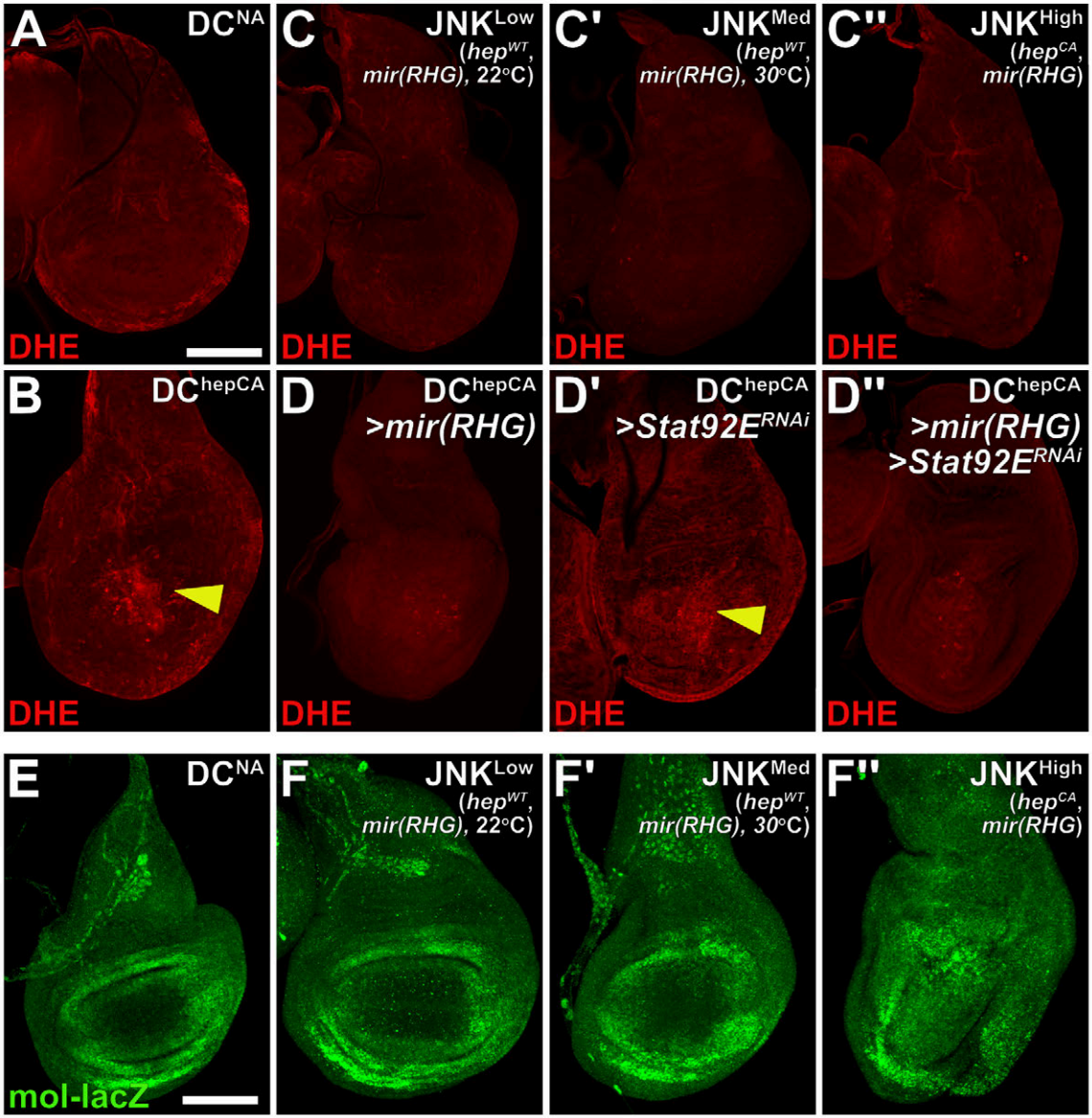
A
DC^NA
DHE
C
JNK^Low
(hep^WT,
mir(RHG), 22°C)
DHE
C'
JNK^Med
(hep^WT,
mir(RHG), 30°C)
DHE
C''
JNK^High
(hep^CA,
mir(RHG)
DHE
B
DC^hepCA
DHE
D
DC^hepCA
>mir(RHG)
DHE
D'
DC^hepCA
>Stat92E^RNAi
DHE
D''
DC^hepCA
>mir(RHG)
>Stat92E^RNAi
DHE
E
DC^NA
mol-lacZ
F
JNK^Low
(hep^WT,
mir(RHG), 22°C)
F'
JNK^Med
(hep^WT,
mir(RHG), 30°C)
F''
JNK^High
(hep^CA,
mir(RHG)